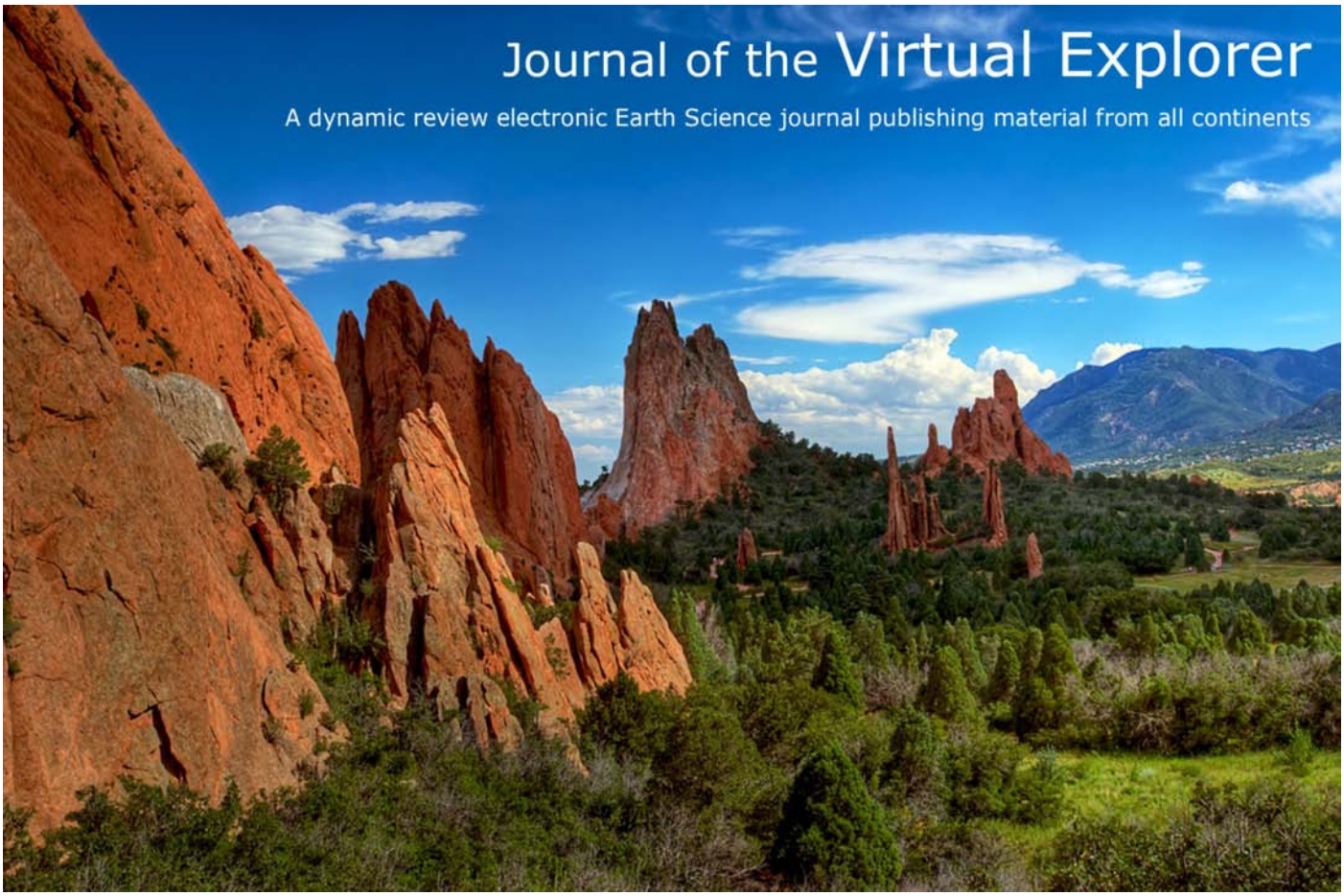

Geology of the Sanctuary of Zeus, Mount Lykaion, Southern Peloponessos, Greece, and Field Guide

George H. Davis

Journal of the Virtual Explorer, Electronic Edition, ISSN 1441-8142, volume **33**, paper 1
In: (Ed.) George H. Davis,
Geology of the Sanctuary of Zeus, Mount Lykaion, Southern Peloponessos, Greece, 2009.

Geology of the Sanctuary of Zeus, Mount Lykaion, Southern Peloponessos, Greece, and Field Guide

George H. Davis

Journal of the Virtual Explorer, Electronic Edition, ISSN 1441-8142, volume **33**, paper 1
In: (Ed.) George H. Davis, Geology of the Sanctuary of Zeus, Mount Lykaion, Southern Peloponessos, Greece, 2009.

Abstract: Detailed structural geological mapping of bedrock and structures within the Sanctuary of Zeus on Mt. Lykaion in the Peloponessos (Greece) reveals intimate ties between the archaeological and geological elements at the site. The physiographic setting of this Pan Hellenic mountaintop sanctuary is dramatic visually. The upper part of the sanctuary is situated on top of a high dome-like summit (~1400 m) known as Agios Elias (St. Elijah). Archaeological elements comprising the lower part of the sanctuary are distributed on a broad rolling surface at the base of Agios Elias on its north and west. The east margin of the upper sanctuary is a precipitous landslide-strewn escarpment actively being shaped by normal faulting related to regional extension. Active normal faults criss-cross the very summit of the sanctuary. The abrupt change in geomorphology from the lower to upper sanctuary areas coincides with the trace of a 10°-easterly dipping thrust fault (the Lykaion thrust fault), which was active in the early Tertiary and accommodated kilometers of east-to-west tectonic transport. The bedrock of Mt. Lykaion comprises five rock formations of the Pindos Group, and each has a very distinctive stratigraphic and landscape signature. The oldest sediments of the Pindos Group were deposited in a deep narrow part of the Neotethyan ocean. Pindos Group deposition began in the Jurassic with a restricted-basin phase in which the Pindos basin was deep, far from shore, and sediment starved. The pre-orogenic history continued through late Cretaceous time, producing overall a sedimentary section ~1000m thick. The preorogenic history ended in latest Cretaceous when the Pindos basin began to be inverted and closed through formation of thrust faults and associated macro-folds. Uplifted blocks shed clastic sediments of latest Cretaceous through Oligocene age. Regionally the synorogenic sequence is ~300m thick and represented primarily by Flysch Transition Beds, which in the Mt. Lykaion area is ~100m in thickness.

Citation: Davis, G. 2009. Geology of the Sanctuary of Zeus, Mount Lykaion, Southern Peloponessos, Greece, and Field Guide. In: (Ed.) George H. Davis, *Journal of the Virtual Explorer*, volume **33**, paper 1, doi: 10.3809/jvirtex.2009.00242

I. INTRODUCTION

The Sanctuary of Zeus, Mt. Lykaion, occupies Agios Elias, the second-highest peak of Mt. Lykaion (Figure 1). At an elevation of ~1360 m, the sanctuary is located ~14 km west of Megalopolis and ~33 km southeast of Olympia in the southern Peloponessos, Greece (Figure 2). The mountaintop summit itself is shaped like a dome, the base of which is a gently rolling bedrock surface that forms a kind of apron along the northern and western margins at an elevation of ~1170 m. Thus, when viewed from north or west, the dome appears to be projecting upward from a pedestal (Figure 3A). In contrast, the eastern margin of the mountaintop summit is a 200 m precipitous drop, strewn with landslides and rock falls. When viewed from the east, therefore, the Sanctuary of Zeus appears daunting and rather inaccessible (Figure 3B).

Figure 1. Summer storm on Mt. Lykaion

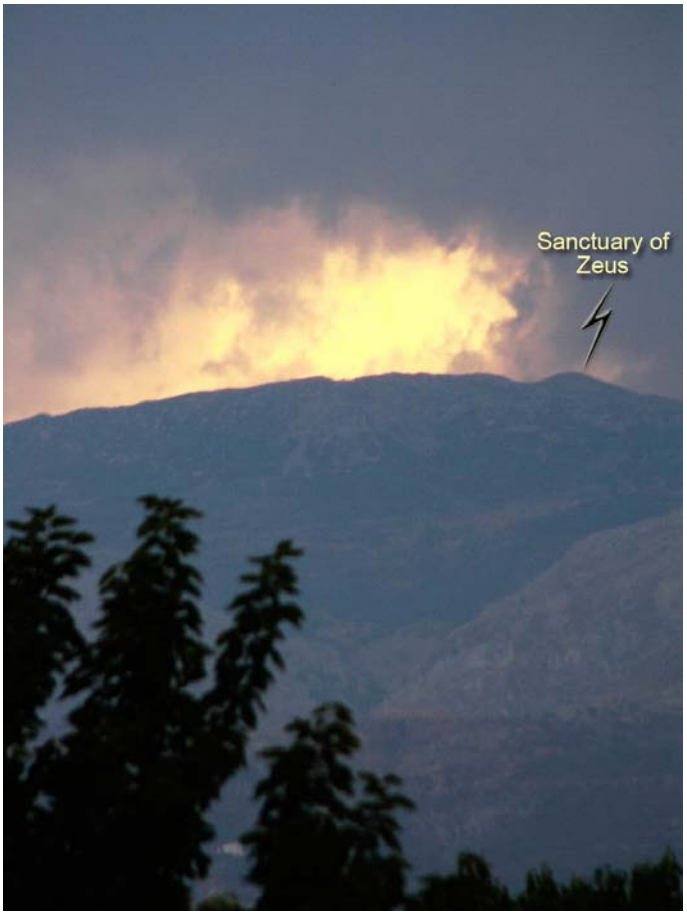

West-directed view of Mt. Lykaion from the city of Megalopolis. A summer storm is raging on the top of this mountain, where the Sanctuary of Zeus ("lightning wielder") is located.

Figure 2. Location map of Mt. Lykaion

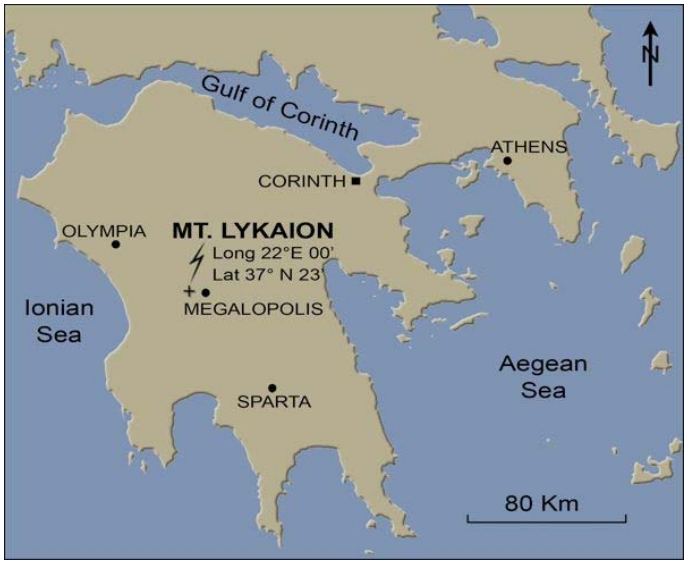

Location map showing the Sanctuary of Zeus, Mt. Lykaion, in Arcadia in the southern Peloponessos. It lies just 30 km southeast of Olympia.

Figure 3. Agios Elias

A. East-directed photograph of the Agios Elias summit of Mt. Lykaion. The ash altar to Zeus is located on the very crest of the summit. The clouds hovering above bring to mind epithets of Zeus, such as "cloud-gathering Zeus," "Zeus the shepherd of the clouds," "master of bright lightning," "bright sky," "bringer of the rain," "bringer of storms," "Zeus of the thunderbolt," "Zeus of lightning," and "Zeus furious and raging." (David Romano, personal communication, 2008).

B. West-directed view of Mt. Lykaion, showing the steep, precipitous escarpment bounding Agios Elias on the east, and revealing rock falls, landslides, and structural terraces progressively stepped down eastward.

Pausanias, a Greek traveler and geographer of the 2nd century AD, provides us with an important glimpse of the Sanctuary of Zeus at Mt. Lykaion. He wrote a ten-book *Description of Greece*, including what he saw and learned about the ancient cultural geography while traveling in Arcadia. For example, Pausanias (8.38.5; 8.38.6; 8.38.7; see Frazer, 1913) makes specific reference to the Sanctuary of Zeus as a sacred place of pan-Hellenic significance, with stadium and hippodrome in which athletic games were held, a sanctuary of Pan, and a temenos and ash altar of Lykaion Zeus. The stadium and hippodrome lie within the lower part of the sanctuary on the flattish bedrock surface; the temenos and ash altar, in contrast, occupy the summit area of Agios Elias (Figure 4B). According to Pausanias (8.38.5; see Frazer, 1913): *"There is on Mount Lykaion a sanctuary of Pan, and a grove of trees around it, with a hippodrome in front of which is a stadion* (Figure 4A). *Of old they used to hold here the Lykaion Games."* Further, Pausanias pointed out (8.38.7, 8.38.6; see Frazer, 1913): "On the highest point of the mountain is a mound of earth, forming an altar of Zeus Lykaios, and from it most of the Peloponessos can be seen" (Figure 4B). "*...On this altar they sacrifice in secret to Lykaion Zeus;*" adding (Pausanias, 8.38.6, see Frazer, 1913) "*...on [Lykaios] is a temenos of Lykaion Zeus, into which people are not allowed to enter. If anyone takes no notice of the rule and enters, he must inevitably live no longer than a year"* .

Figure 4. Hippodrome and ash altar

A. South-directed view of hippodrome (flat grassy area in foreground and middle ground). White limestone blocks and structures in far left in middle ground are part of stoa and fountain complex. Road slanting up to the right in background essentially follows Lykaion thrust fault.

B. North-directed view showing ash altar (being excavated) on Agios Elias in the foreground and the view of the Peloponessos in the background.

It needs to be emphasized that the Sanctuary of Zeus on Agios Elias is truly a mountaintop sanctuary, and many of those who made the pilgrimage to the Sanctuary of Zeus experienced a long journey even before coming to the lower sanctuary. We know from a stone-slab (stela) record of the names of victors of the 304/03 B.C. Lykaion games that athletes hailed from long distances away from Mt. Lykaion, *e.g.*, Macedonia, Syracuse, Rhodes, and broad reaches of Arcadia (Romano, 1997). Most may have come to Lykaion through Megalopolis, and

ascended to the sanctuary from there. Megalopolis (see Figure 2) is located in a broad low basin created by active extensional faulting, one that for millions of years was a closed depression in which swampy conditions prevailed. Pausanias described Megalopolis as *"gateway to the marsh;"* today the city sits next to a gigantic open-pit lignite operation. Traveling from Megalopolis to the Lykaion summit required a walk of ~25 km and an ascent of more than 900 m, and this was 'just' the final chapter of the pilgrimage.

II. PURPOSE OF THIS PAPER

The Sanctuary of Zeus, Mt. Lykaion, is the object of investigation of the Mt. Lykaion Excavation and Survey Project, jointly led by Dr. David Romano (The University of Pennsylvania Museum of Archaeology and Anthropology), Dr. Mary Voyatzis (Department of Classics, The University of Arizona), and the Thirty-Ninth Ephorate of Prehistoric and Classical Antiquities at Tripolis, under the auspices of The American School of Classical Studies at Athens (http://lykaionexcavation.org/).

Scant archaeological excavation preceded the Mt. Lykaion Excavation and Survey Project, which was initiated in 2004. The notable exception was the work by K. Kourouniotes (1903; 1904; 1905; 1909), whose investigations are summarized by Romano (http://lykaionexcavation.org/). Kourouniotes excavated in several parts of the sanctuary in 1897, 1902, and 1906. The finds he recovered (*e.g.*, coins, pottery, figurines) showed that activity at the altar dated back to as early as the late 7th century BC, but peak activity was during the Classical period.

David Gilman Romano (1997) built upon the work of Kourouniotes and conducted an architectural and topographical survey at the site. He mapped the various archaeological elements, a simplified rendition of which is shown in Figure 5: a lower part with the hippodrome (horse- and chariot-racing track), stadium (located *within* the hippodrome), bath, xenon (lodging place for those who came from afar), stoa (connected porticos under one roof), and the Agno fountain (a once very productive spring); and an upper part with temenos (sacred precinct), column bases, and an ash altar (place of sacrifice of animals and dedications of offerings) (Figure 3). Romano (1981, 1997) concluded that the stadium was one of the most important in the Greek world, and noted the hippodrome on Mt. Lykaion is the only extant and visible example throughout the Greek world.

Figure 5. Topographic map of Sanctuary of Zeus, showing archaeological elements

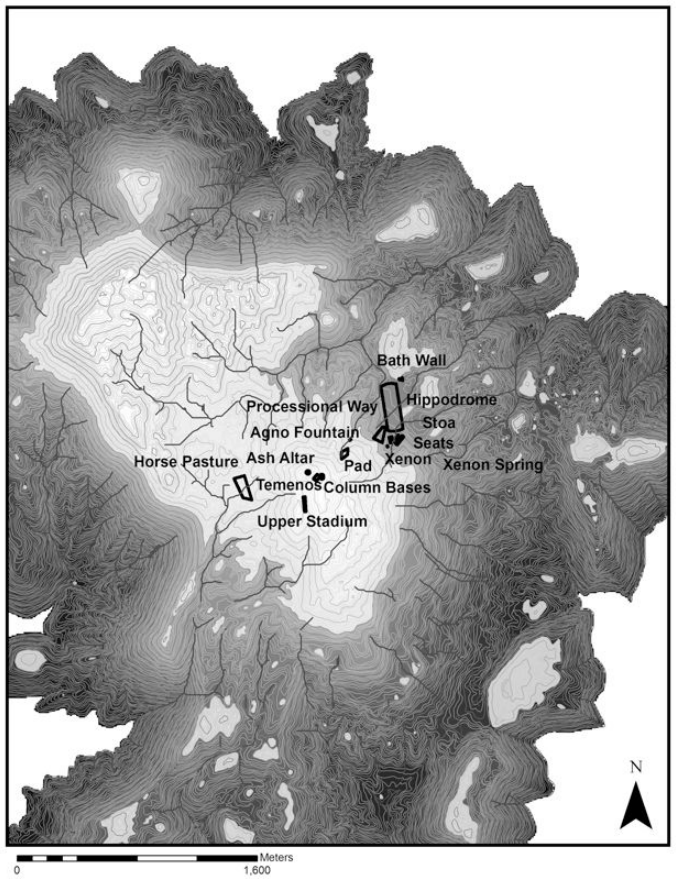

Topographic map of the summit area showing the chief archaeological elements within the Sanctuary of Zeus on Mt. Lykaion. Contour interval is 4 m. The white areas are the highest ground. The dark areas dramatize the steep drop-off on all sides from the Sanctuary of Zeus. This map is based on the work of Romano (1997; and ongoing).

When the Mt. Lykaion Excavation and Survey Project was initiated, I was invited by Dr. Romano and Dr. Voyatzis to carry out geological investigations that would inform interpretation of history and archaeology. The only prior geological investigations that touched upon this area was the regional geological mapping carried out by Lalchos (1973), who produced the Kato Fighalia Sheet at a scale of 1:50,000, and by Papadopoulous (1997), who produced the Megalopolis Sheet, also at a scale of 1:50,000. No reports or articles accompanied this mapping. Furthermore, no detailed investigations had ever been carried out within the Sanctuary of Zeus proper. I have carried out geological mapping during the summers of 2004, 2005, 2007, 2008 and 2009 (total of 16 weeks overall). The limits of the Sanctuary of Zeus *per se* are

somewhat arbitrarily defined, but all of the archaeological elements occupy comfortably an area of 1.5 km^2. I found it necessary to map a significantly larger area (~25 km^2) in order gain fuller perspective of the subregion within which the site is located, and to be able to trace critical contacts into the sanctuary site. Thus the map area described in this paper occupies an area of, which I mapped in great detail at a scale of ~1:6000.

The emphasis of this paper is on the overall geology of the Sanctuary of Zeus, but with a particular focus on structural geology and tectonics. It concludes with a geological field guide to the area (Appendix A). Other manuscripts that I am preparing will emphasize to a greater degree the geoarchaeological dimensions of the Sanctuary of Zeus, and these will become useful companion pieces to the fundamental geological descriptions, observations, interpretations, figures, and maps contained in this contribution.

Please note that all headings in the manuscript are denoted in Times New Roman (*e.g.*, VI-A). This is to create ease of cross-referencing from the field trip guide to supporting facts and interpretations in the body of this text.

III. PLATE TECTONIC SETTING

The contemporary plate tectonic setting of the Aegean has been well researched. Based on results of Global Positioning System (GPS) geodesy, Greece itself, embedded within the Aegean tectonic plate, is known to be moving S40°W at a rate that from place to place ranges from 2 cm/yr to nearly 4 cm/yr (Le Pichon and others, 1995; Oral and others, 1995; Reilinger and others, 1997; Cocard and others, 1999; McClusky and others, 2000) (Figure 6). Mt. Lykaion, in particular, moves 3.7 cm to the southwest each year. The sustained plate movement is the result of simultaneous *push* and *pull* forces affecting the entire eastern Mediterranean region. The push comes from the northeast, where the Anatolian tectonic plate is being squeezed westward into the Aegean region by the slow-motion (2 cm/yr) ramming of the Arabian plate into Turkey (McKenzie, 1970; Reilinger and others, 1997). The pull comes from the south, where along the seismically active Hellenic trench the African plate is subducting under the Aegean crust (*e.g.*, Jackson, 1994). The subducting African plate is foundering in such a way that a suction force is created, which pulls the Aegean plate toward it and increases the velocity of movement to 4 cm/yr (Reilinger and others, 1997).

Figure 6. Plate setting and GPS velocity vectors for Eastern Mediterranean.

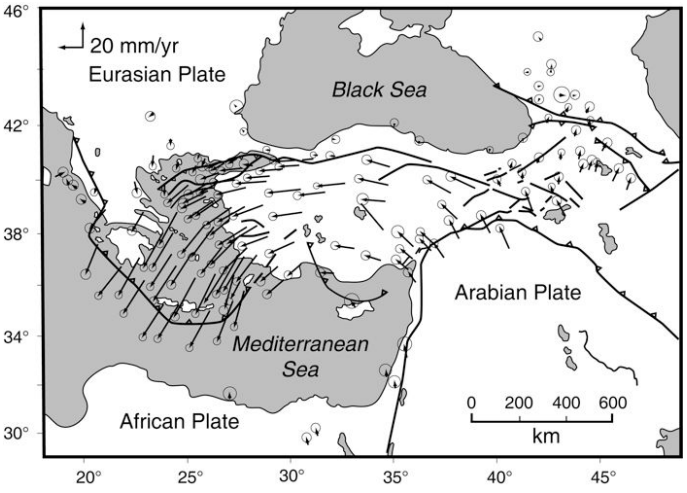

Global Positioning System (GPS) map showing velocity vectors for reference stations. From McCluskey and others, 2000, figure 2, p. 5703.

With northern Greece moving 2 cm/yr southwesterly, and southern Greece moving nearly twice as fast, the region finds itself being actively stretched, and thus thinned, tectonically (McKenzie, 1978; Jackson and others, 1982; Jackson, 1994; Clarke and others, 1998). The Gulf of Corinth is a dramatic example of the stretching (Jackson and others, 1982; Roberts and Stewart, 1994; Roberts, 1996; Briole and others, 2000; Sorel, 2000; Morewood and Roberts, 2001). Abundant normal faulting accommodates the extension. This faulting has been described and documented by many workers, including Roberts and Jackson (1991), Stewart and Hancock (1991), Jackson (1994), Jackson and McKenzie (1999), Roberts and Ganas (2000), and Goldsworthy, Jackson, and Haines (2002). Van Hinsbergen and others (2006) emphasized that the present-day extensional deformation, which is producing the normal faulting, began in the late Pliocene in southern Greece. The Cyclades islands disclose the results of profound subsidence over a vast region in the past 20 million years (Lister and others, 1984; Jolivet and Patriat, 1999; Jolivet and others, 2004).

A fundamental expression of the fault activity is the blizzard of earthquake activity that Greece experiences continuously (Ambraseys and Jackson, 1990, 1998; Jackson, 1994; Reilinger and others, 1997, see Figure 2, p. 9985; McClusky and others, 2000; and Morewood and Roberts, 2001). The Aegean region is *very* active seismically. Fault-plane solutions are varied, but include

abundant earthquakes related to active normal faulting, *i.e.*, faults accommodating the crustal stretching. Ambraseys and Jackson (1990) reviewed all earthquakes of magnitude 5.8 and greater that had occurred in Greece, and concluded that the cumulative displacements can account for a total north-south stretching of Greece by ~45-70 cm during that time interval.

Mt. Lykaion has not escaped the earthquake activity caused by the active extension. A revealing example is the devastating Megalopolis earthquake (Ms = 5.9) of April, 1965), which caused extensive damage to our host village, Ano Karyes, as well as surrounding villages (Ambraseys, 1967; Ambraseys and Jackson, 1998). The epicenter of this earthquake was merely 4 km northwest of Mt. Lykaion (Figure 7). It appears to have occurred at shallow depth, approximately 10 km below the surface (Ambraseys, 1967; Ambraseys and Jackson, 1998). Its effects were felt within a 300,000 sq km area of the Peloponessos, killing 20 people and injuring 160. Of the 99,000 houses in the affected region, 110 collapsed, 5000 were damaged beyond repair, 6000 were damaged seriously, and 7000 were slightly damaged (Ambraseys, 1967). Ambraseys (1967, p. 1030) described how accelerations were amplified in landslide areas, emphasizing high number and large sizes of slides either created for the first time or reactivated by the shock. Indeed, a part of the village of Ano Karyes, the base of operations for the Mt. Lykaion Excavation and Survey Project, is built on an extensive array of landslide deposits, and some houses were badly damaged.

Figure 7. Map showing impact of Megalopolis earthquake.

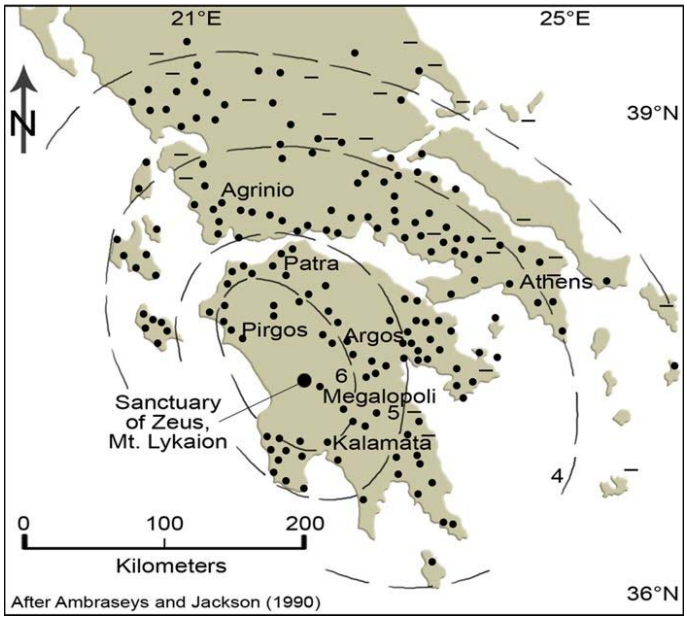

Map representing The April 5, 1965 Megalopolis earthquake (M_S5.9). Note location of the Sanctuary of Zeus. The epicenter of this earthquake was located 4 km northwest of the sanctuary. Contours represent lines of equal intensity of ground shaking, as deduced from documentation of damage on the ground. Magnitudes of intensity are in relation to the Modified Mercalli Scale: VI = felt by everyone, and people run outdoors; some heavy furniture moved, chimneys become damaged, plaster falls. III = felt quite noticeably indoors, especially on upper floors of building, but many people do not recognize it as an earthquake. From Ambraseys and Jackson, 1990, figure A40, p. 702.

IV. REGIONAL TECTONIC SETTING

Understanding the nature and origin of the sedimentary rocks exposed on Mt. Lykaion requires examining the Triassic through Eocene regional tectonic history of this part of the Aegean region (Robertson and Dixon, 1984; Golonka, 2004). Prior to approximately middle Triassic (~210 Ma), the regions we now refer to as northern Africa, southwestern Europe, and northeastern North America were close neighbors within the Pangaea super continent. The rifting apart of Pangaea then took place, and the North Atlantic began to open (Degnan and Robertson, 1998). Major faults associated with the rifting broke eastward to the Neotethyan Ocean. Within a part of the Neotethyan Ocean, a very deep, narrow (~160 km wide) oceanic basin opened up, known as the Pindos basin (Pe-Piper and Piper, 1984; Degnan and Robertson, 1998; Piper, 2006). In it was deposited a sequence of sedimentary

rocks of Late Triassic (~200 Ma) through late Oligocene (~25 Ma) age. These now comprise the "Pindos Group" stratigraphy of mainland Greece and the western Peloponessos (Degnan and Robertson, 1998; Skourlis and Doutsos, 2003). Not all of the stratigraphy of the Pindos Group is represented at Mt. Lykaion, but the sequence is reasonably complete, with units as old as mid-Jurassic (~180 Ma) and as young as late Eocene (~34 Ma).

Two different tectonic conditions are revealed in the Pindos Group stratigraphy of the Peloponessos (Degnan and Robertson, 1998). Rocks in the lower part of the Pindos Group, which range in age from latest Triassic (~210 Ma) to latest Cretaceous (~65 Ma), are preorogenic and reveal a period during which the Pindos Basin was deep, far from shore, sediment starved, and slowly accumulating the tests of pelagic organisms that accumulated in silica- and carbonate-rich mud and ooze (Bosellin and Winterer, 1975; Baltuck, 1982). From time to time this basin received influxes of carbonate-rich debris flows propelled from the basin margin(s) down the continental slope to the abyssal depths via turbidity currents (Richter and Mueller, 1993; Walgreich and others, 1996; Avramidis and Zelididis, 2001; Degnan and Robertson, 1994, 2006).

Rocks in the upper part of the Pindos Group, which range in age from early Paleocene (~64 Ma) to latest Oligocene (~25 Ma), are synorogenic, and reveal a period in which the Pindos basin was being closed and tectonically inverted into a mountain through faulting and folding (van Hinsbergen and others, 2006, see Figure 14, p. 483). Turbidity currents moved sediments from the basin margin(s) to the ocean floor, this time in the form of sand, silt, and mud derived from erosion of uplifts created by faulting and folding (van Hinsbergen and others, 2005). Thus Pindos Group limestones in the upper part of the stratigraphic column become dominated by large influxes of sandstones derived from the tectonically uplifted parts of the closing basin. The thickness of the pre-orogenic sedimentary section throughout most of the Pindos Group is ~1000 m; the thickness of the syn-orogenic sedimentary section in the Peloponessos is ~300m, though becoming much thicker to the north of the Gulf of Corinth (Skourlis and Doutsos, 2003).

V. THE PINDOS FOLD AND THRUST BELT

Tectonic inversion of the Pindos basin was achieved by compression-induced shortening, which created the Pindos fold-and-thrust belt, a belt that can be traced north-south through western Greece (Wagreich and others, 1996; Doutsos and others, 2000; Skourlis and Doutsos, 2003) (Figure 8). The Pindos sedimentary sequence experienced significant shortening (Degnan and Robertson, 1998; Doutsos and others, 2000; Skourlis and Doutsos, 2003) (Figure 9A). Based on detailed geological mapping and analysis of folds and thrust faults within the Pindos belt overall, Skourlis and Doutsos (2003) concluded that tectonic shortening in excess of 50% was achieved through a combination of layer-parallel shortening, thrust faulting, and buckling (Figure 9B). The net effect was fault imbrication of the sedimentary sequence. Strata within each panel became folded in a way determined by the shapes of the major thrust faults along which the beds were transported and the distance of tectonic transport, typically measured in kilometers. During thrusting and folding, the Pindos Group strata were structurally thickened, and became elevated.

Figure 8. Map of tectonic provinces in Greece.

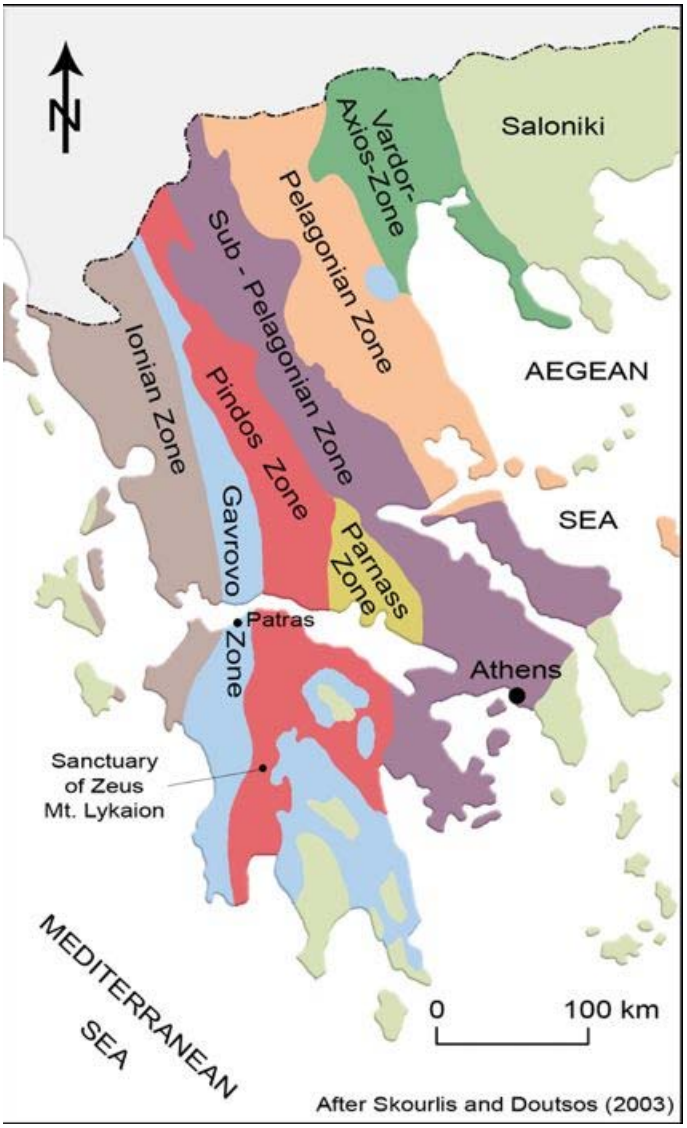

Map showing the Pindos fold-and-thrust belt, which runs north-south across all of Greece. Adapted from Walreich and others, 1996, figure 1, p. 325.

Figure 9. Pindos Belt folding and thrusting.

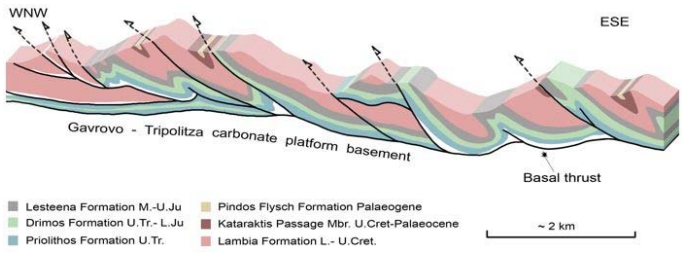

A. Structure section showing overall style of deformation by thrust faulting and folding in the Pindos Zone fold and thrust belt. From Degnan and Robertson, 1998, figure 3, p. 37).

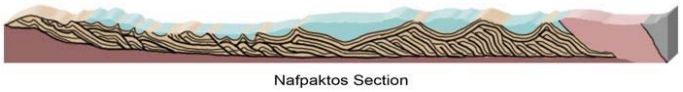

B. Structure section showing the details of thrust faulting, imbrication, and folding. This is an east-west structure section that crosses the Pindos fold and thrust belt just north of the Gulf of Corinth in the Navpatkos region. From Skourlis and Doutsos, 2003, figure 3, p. 895.

The resulting Pindos mountain system, as it emerged, became subject to erosion, with the erosion-derived sediments transported by streams and currents to sites of both non-marine and marine deposition. The sediment influxes contributed to forming the syn-orogenic sediments that became the upper part of the Pindos Group (Walgreich and others, 1996; van Hinsbergen and others, 2005; Degnan and Robertson, 2006; and Piper, 2006). As the Pindos basin continued to close, folding and thrusting shortened these freshly minted sediments as well.

The direction of tectonic transport within the belt was from ENE to WSW, along a line perpendicular to the overall NNW/SSE trend of the Pindos fold-and-thrust belt (Degnan and Robertson, 1998; Skourlis and Doutsos, 2003). The thrust panels of Pindos Group sedimentary rocks are allochthonous and now reside tens of kilometers west of where they were originally deposited (van Hinsbergen and others, 2005). But the story is even more complicated. Following the tectonic development of the Pindos fold-and-thrust belt, the whole belt experienced a 50º clockwise (vertical axis) rotation. Restoring the rotation makes it clear that the original tectonic transport direction for the Pindos belt actually was north to south.

VI. STRATIGRAPHY WITHIN THE SANCTUARY OF MT. LYKAION

VI-A. Previous Work

The geology of the subregion within which the Sanctuary of Zeus resides was originally mapped (1:50,000 scale) by Lalechos (1973) and Papadopoulos (1997). The full aerial dimensions of their mapping (~2,000 km^2) far exceeded those of the Mt. Lykaion Sanctuary area proper (~1. 5 km^2), and the aerial extent of my own mapping to date (~25 km^2), which reaches out beyond the sanctuary in order to gain broader perspective. Lalechos (1973) and Papadopoulos (1997) described the nature of the lithologies and fossil assemblages within each of four Pindos

Group formations they recognized: Chert Series Jurassic to Lower Cretaceous), First Flysch (Upper Cretaceous), Limestones (Upper Cretaceous), and Flysch Transition Beds (Paleocene to Eocene) (see descriptions, Appendix B).

With only modest adjustments in the names and subdivision, I basically adopted the map units established by Lalechos (1973) and Papadopoulos (1997) (Figure 10). From oldest to youngest the units are as follows: Chert Series Beds, First Flysch Beds, Thin Platy Limestone Beds, Thick White Limestone Beds, and Flysch Transition Beds. It proved useful from a mapping and structural geologic standpoint to split the Limestones formation (Lalechos, 1973; Papadopoulos, 1994; see Appendix B) into two members: a lower member, which I refer to as *"Thin Platy Limestone Beds,"* and an upper member, which I call *"Thick White Limestone Beds"* (see Figure 10). Descriptions that follow emphasize the outcrop-scale properties.

Figure 10. Stratigraphic column for study area.

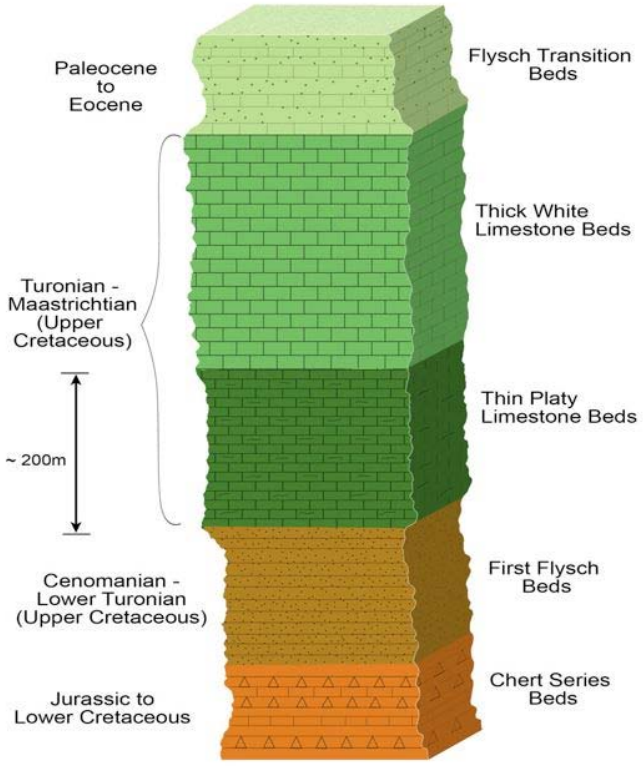

Stratigraphic column showing formations of the Pindos Group exposed in the Sanctuary of Zeus study area. These units were defined during the course of this study, modified very slightly from the work of Lalechos (1973) and Papadopoulos (1997). "Limestones" of Lalechos (1973) and Papadopoulos (1997) are subdivided here into a lower unit ("Thin Platy Limestone Beds"), and an upper member ("Thick White Limestone Beds"). The contact between these two members is transitional over a thickness of ~20 m, where typical Thin Platy Limestone Beds alternate with typical Thick White Limestone Beds. Furthermore, "First Flysch" of Lalechos (1973) and Papadopoulos (1997) is referred to here as "First Flysch Beds," and subdivided into a lower member ("Lower Brown Sandstone"), an upper member ("Upper Brown Sandstone"), and a middle member ("Red Mudstone") in between.

VI-B. Chert Series Beds

The Chert Series Beds comprises a formation that ranges up to 100 m in thickness (see Figures 8), which is also the thickness reported by Lalechos (1973) and Papadopoulos (1997) (see Appendix B). The thin-bedded radiolarian cherts, and interbedded limestones and sandstones that make up this formation tend to be very poorly exposed. This formation is a slope former, which reflects the vulnerability of its sheared and broken character to weathering and erosion. Yet certain outstanding road-cut exposures reveal diagnostic characteristics.

One of the most distinctive expressions of the Chert Series Beds is the presence of red-purple, thin-bedded ribbon cherts (Figure 11A). Individual chert "ribbons" are typically 5 to 10cm thick and marked by very closely spaced (up to 6 cm) systematically oriented fractures (joints) that are omnipresent (see Figure 11A). The ribbon cherts are interbedded with reddish-brown and with light gray limestone interbeds (generally up to 1 m thick). The mudstones are commonly pervasively sheared (Figure 11B), especially where found in close proximity to major thrust faults. Limestone interbeds commonly display tight folding of a strongly overturned to recumbent nature (Figure 11C). Brown sandstones (generally up to several meters thick) are common within the Chert Series Beds as well. The Chert Series Beds accumulations are importantly composed of the tests of calcite-forming and silica-forming protozoans (foraminifera and radiolarian, respectively). Before dying and descending to become muddy ooze, these protozoans floated in pelagic-zone ocean waters far away from shore and 2 kms or more above the seafloor bottom in which they ultimately accumulated.

Figure 11. Outcrop expressions in Chert Series Beds

(A) Ribbon beds of radiolarian chert with layer-perpendicular closely spaced joints. Field notebook for scale.

(B) Sheared red mudstones within Chert Series Beds.

(C) Recumbent isoclinal fold in limestone layers, within radiolarian chert and mudstone sequence. Thickness of limestone layer (light gray) at base of outcrop is ~12 cm.

Lithologies within the Chert Series Beds are quite incompetent. Clearly this formation was exploited preferentially by thrust faulting and thrust shearing, offering very little resistance to compression-induced deformation, and increasing the ease with which thrust sheets were transported. The outcrop presence of Chert Series Beds is in places signaled by the presence of 'sparkles' on the ground, which prove to be tiny (0.5 cm X 0.5 cm and smaller) chips and flakes of siltstone, chert, and mudstone with phyllonitic surfaces produced during thrusting and shearing. The thin phyllonitic selvages are, in effect, tectonically polished bedding surfaces. From place to place there are also tectonic inclusions of spindle-shaped rock fragments (generally up to 7 cm in length), smoothed and polished through thrust shearing. The stratigraphic and structural position of Chert Series Beds has been depicted by Degnan and Roberson (1998) along sole thrusts (see Figure 9A), and this underscores the degree to which this formation was exploited geomechanically during thrusting.

The structural character of outcrops of Chert Series Beds is strongly influenced by marked contrasts in mechanical behavior. On the one hand there are the ribbon-chert layers, which in response to deformation became pervasively and systematically jointed (see Figure 11A). The joints tend to be perpendicular to bedding and spaced at intervals commonly less than bedding thickness. The result is a fracturing that, in places, resembles cleavage, and is so distinctive that the fracturing itself is a criterion for recognizing Chert Series Beds. As noted above, the brittle ribbon chert layers typically are interbedded with incompetent mudstones, and where such packages were shortened the chert layers accommodated buckling and free folding within the more ductile encompassing matrix. Some folds are upright anticlines and synclines, while others are overturned to recumbent, and in places detached through transposition in ways that outcrops reveal isolated fold hinges (see Figure 11C). Where sandstone beds crop out in the Chert Series Beds exposures, they tend to be jointed and fractured, but rarely folded. Overall the Chert Series Beds are intensely sheared, and in places have deconstructed to sticky fault gouge and quasi-foliated tectonites.

Small joint-bounded specimens of Chert Series Beds are miniature textbook displays of joint properties, including hackles, ribs, and en echelon fringe joints (Figure 12). Future work will evaluate jointing systematics

within the Chert Series Beds in relation to Pindos-belt folding and thrusting.

Figure 12. Photograph of jointed specimens of bedded chert from the Chert Series Beds

A. The upper and lower surfaces of this cube of ribbon chert correspond to bedding. The flanks of this cube are joint surfaces. Even spacing of jointing and bedding, and the orthogonal character of the joint sets resulted in 'cubic' weathering.

B. This wedge of chert has steep faces marked by jointing, and horizontal surfaces defined by bedding. Delicate fringes of joint surfaces are displayed by samples such as this.

C. Part of a joint face in chert. The curved lines are traces of ribs. Tiny delicate hackles are evident in places along the ribs, and are especially pronounced where there is manganese staining.

D. Very closely spaced, penetrative joining in chert, giving a sense of the very brittle nature of this rock.

VI-C. First Flysch Beds

The First Flysch Beds comprise a unit that ranges up to 155 m in thickness (see Figure 10), which is greater than the 100 m figure reported by Lalechos (1973) and Papadopoulos (1997) (see Appendix B). It is, overall, a slope-forming unit, but projecting from the moderately steep slopes there tend to be large smooth knobs and/or blocky bedrock projections (up to 10 m in topographic relief) of more resistant bedrock (Figure 13). The dominant rock type is brown sandstone, and it would be easy to assume, though falsely, that the entire formation is composed of sandstone. However, detailed geological mapping revealed an internal stratigraphy marked by upper and lower brown sandstone members 'sandwiching' a middle red-mudstone member. Both the upper and lower members (strictly informal designations) are composed of massive brown sandstone ranging up to 60 m and 75 m, respectively, and consisting of thick beds (up to 4 m) within a rather homogenous stratigraphic succession. The red mudstone member appear to range up to ~20 m in thickness. The red mudstone is very poorly exposed, but its presence can be inferred from reddish colluvium.

Figure 13. Sandstone outcrops of First Flysch Beds, behind spring.

Note the generally fractured character of the sandstone. First Flysch Beds rest on Chert Series Beds, which, due to shearing, create an impermeable 'seal' beneath the Chert Series Beds at this location. As a result, ground water within the First Flysch Beds seeps out along the spring which is evident in the foreground.

The massiveness of the brown sandstone members does not lend itself it folding. Instead, the dominant outcrop-scale structural characteristic is jointing, typically with a spacing of one or two meters. Jointing is not systematic in outcrop, neither in orientation or spacing. Instead, the jointing commonly has the appearance of irregular fracturing (Figure 14), with apparent wide-ranging orientations of the fractures and the presence of abundant curviplanar fractures.

Figure 14. Fractured sandstone of First Flysch Beds.

Outcrop expression of fracturing and jointing within sandstone of the First Flysch Beds.

Wagreich and others (1996, p. 328) emphasized that First Flysch sediments represent the first appearance of sandstones and siltstones in the deep-water Pindos basin. The shift to sandstone deposition may have occurred as a result of sea-level fall and the formation of incised valleys in the basin shelf, which became avenues for transporting the clastic material into the deeper waters (Wagreich and others, 1996).

VI-D. Thin Platy Limestone Beds

Thin Platy Limestone Beds is a formation approximately 170 m thick (see Figure 10). It is homogenous in its geological properties, consisting of even-bedded, platy limestone, with thickness of individual beds typically ranging between 20 cm and 35 cm (Figure 15A). The appearance of the thick sequence of limestone signals a shelf margin of the Pindos Basin rich in carbonate platforms. Large volumes of eroded carbonate debris would periodically be carried via submarine turbidity currents down the slope, creating limestone deposits on the basin bottom (Degnan and Robertson, 1998).

Figure 15. Photographs of outcrop character of Thin Platy Limestone Beds

A. Typical even-bedded, thin-bedded limestone with concordant chert layers, which in this example are white. Chert layers in this outcrop are ~10 to 15 cm thick.

B. Here the limestone displays the typical combination of thin bedding, closely spaced fracturing, and chevron folding. Compass barely visible near center of photograph, at base of prominent white limestone bed in lower limb.

C. Because the thickness of bedding and the spacing of fractures are essentially the same, weathering and erosion of this formation creates a blocky, 'cider-block' appearance.

Fractures (joints) are abundant in Thin Platy Limestone Beds, in the form of planar, parallel surfaces that cut nearly perpendicular to bedding and spaced typically 20 to 40 cm apart (Figure 15B). The limestone is light to medium gray in color. This gray tone is embellished by the presence of both black and white chert nodules and layers that abundantly occur within the Thin Platy Limestone.

Displays of Thin Platy Limestone Beds in roadcuts are quite inviting, displaying ubiquitous chevron fold structures (commonly overturned) and the eye-catching combination of limestone and chert (see Figure 15B). The fold forms are ones whose geometric and structural properties are derived from the flexural-slip mechanism of folding (Ramsay, 1974). Thin mudstone and claystone layers (up to several centimeters in thickness) commonly separate the limestone beds from one another, thus revealing that the frictional resistance to slip along bedding planes may have been vanishingly small during folding. In the creases of the folds the effects of tight compression are evident, both in the local presence of tectonic stylolites and fiber veins.

Roadcut exposures of the Thin Platy Limestone Beds give the impression that this formation, dominated by competent limestone and chert, should boldly crop out in the general landscape and thus be a cliff- or bench former. Ironically, this is not generally the case. Instead, hill slopes underlain by Thin Platy Limestone Beds either are smoothly eroded (topped by soil and brushy vegetation) or covered in rubble and scree in the form of limestone blocks, about the size of cinder blocks. This characteristic weathering is attributable here to bedding thickness and fracture spacing being essentially the same within this formation. Thus from a macro view the Thin Platy Limestone Beds is a formation composed of billions of tiny polygonal blocks (Figure 15C), which work themselves loose by the action of thermal expansion and contraction (during freezing and thawing) along with the general effects of water moving along the cracks, goats trafficking up and down the hill slopes, and gravity relentlessly tugging at the slopes

VI-E. Thick White Limestone Beds

The Thick White Limestone Beds comprises a formation that ranges up to ~300 m in the study area (see Figure 10). Although Lalechos (1973) and Papadopoulos (1997) reported 200 m as the maximum thickness of their Limestones unit in the sheets they mapped (see Appendix B), the total thickness of their Limestones unit as estimated here is ~520 m, which includes the sum of thicknesses of the Thin Platy Limestone Beds and the Thick White Limestone Beds.

Thick White Limestone Beds is very distinctive (Figure 16A) and, like the Thin Platy Limestone Beds, is uniform in its characteristic properties. The basic elements throughout the formation are bright white limestone beds that tend to range from 1-4 m in thickness, which is a bedding thickness distinctively greater than that of the Thin Platy Limestone Beds. The contact between Thin Platy Limestone Beds and Thick White Limestone Beds is a transitional sequence, no thicker than ~50m, consisting of an interbedding of the characteristic rock properties of each formation.

Figure 16. Photographs of outcrops of Thick White Limestone Beds

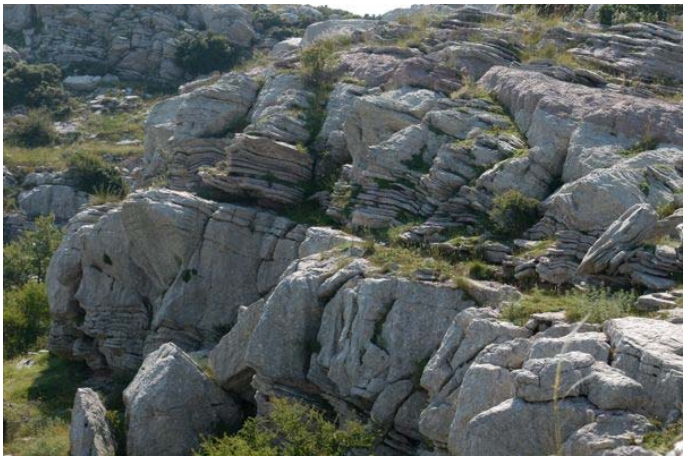

A. Good example of the bench- and cliff-forming nature of this resistant limestone formation. Lower massive layer is ~5m thick.

B. Bold exposures of Thick White Limestone Beds. Vegetation at this location was burned away during the fires of the summer of 2007. Note geologist (Phil Nickerson) in upper right hand corner of photograph.

The physical expression of Thick White Limestone Beds is conspicuous and easily recognized in the landscape, particularly given the bright white massive outcrops. Commonly this formation is abundantly covered with tough shrubs, bushes, and trees, in part because the ruggedness of the projecting and protruding thick white layers of sharp and resistant limestone outcrops does not lend itself to land clearing and/or terracing, nor to efficient goat grazing. The fires of 2007 locally had the effect of "clearing" some of the vegetation, creating even fuller exposures of the resistant Thick White Limestone Beds (Figure 16B). Furthermore, the Thick White Limestone Beds is ubiquitously and beautifully folded (Figure 17), commonly in the form of upright to slightly asymmetrical anticlines and synclines. Even where not folded, the bedding typically is marked by broad, gentle undulations (see Figure 16B).

Figure 17. Photographs of folding within Thick White Limestone Beds

A. Upright anticlines and synclines in the lower part of the Thick White Limestone Beds. Tom Fenn's hand-held GPS receiver is catching satellite signals. Road to Agios Elios in background. View to the southeast.

B. Beautiful small-scale folding of the limestones. Note clipboard for scale.

C. More upright anticlines and synclines. Randy Goosen is the geologist on the crest of one of the chevron anticlines.

One of the peculiar but diagnostic characteristics of Thick White Limestone Beds is the presence of what I refer to as "stylobedding," which is a type of pseudobedding. An example is shown in Figure 17B, where proper bedding planes do not exist, and instead there are bedding-parallel surfaces that are quite tightly curviplanar in detail, and which have been attacked by significant differential weathering and erosion. Another really good example is pictured in Figure 18, where folded "bedding" in a large mass of limestone float is actually folded pseudobedding. Stylolites are the controlling structure, and these are concordant to bedding and reflect an origin of pressure dissolution during burial and compaction within the deep Pindos Basin. I refer to these as "bedding stylolites" as opposed to "tectonic stylolites." Stylolitic teeth and cones are oriented perpendicular to bedding. Fresh exposures of stylolites in this formation can be seen at the Temple of Apollo at Bassai, which lies just 5 km west of Mt. Lykaion. As part of restoration engineering, modern masons are cutting and fashioning blocks of Thick White Limestone Beds there, and thus creating fresh exposures of the limestone and stylolites contained therein (Figure 19A). The original drums and blocks in the Temple of Apollo at Bassai display the stylolites in a very prominent manner, and these patterns of stylolites, in my view, add to the beauty of the architecture (Figure 19B). All of the blocks comprising the remains of built structures within the Sanctuary of Zeus (*e.g.*, stoa, baths, seatwall, xenon, column bases, fountain house, …) are derived from the Thick White Limestone Beds formation, for its thick-bedded nature and strength made it the best suited raw material for such purposes (Figure 19C). Probably none of the other formations would have worked

Figure 18. Float block of tightly-folded stylobedding in Thick White Limestone Beds.

Example of stylobedding in a large mass of limestone float. The rock looks as if someone outlined the 'bedding' surfaces with a black magic marker, so prominent are the weathered and eroded stylolitic surfaces.

Figure 19. Stylolites in Thick White Limestone Beds.

A. Fresh exposure of stylolites in a block of Thick White Limestone Beds. The locale is the Temple of Apollo at Bassai, where restoration work is taking place and new building blocks are being created. The stylolite seams are marked by characteristic teeth and cones, and are lined by insoluble residue (dark seams). The fact that stylolites develop through pressure-solution loss of material is quite apparent, for a limestone vein is cut in several places by stylolites, and dissolution along these has created the offsets of the vein.

B. Ancient drums and blocks at Bassai were chiseled from Thick White Limestone Beds and display the character and penetrative nature of stylolites, the control for pseudobedding.

C. All of the blocks in the built structures at the Sanctuary of Zeus at Mt. Lykaion are derived from Thick White Limestone Beds. In this case we see one of the

column bases just east of the temenos in the upper part of the sanctuary. In fact, Pausanias (8.38.7) referred to the columns: *"Before the altar on the east stand two pillars, on which there were of old gilded eagles."*

VI-F. Flysch Transition Beds

The Flysch Transition Beds (see Figure 10) represents the youngest formation in the area, with a thickness difficult to estimate confidently (at this time) because of the abundance of internal folding. Lalechos (1973) and Papadopoulos (1997) estimate its thickness at 50 m (see Appendix B), but mapping carried out in this study suggests that it may be as thick as 100 m or more. Turbidites within the Flysch Transition Beds are the products of submarine debris flow propelled by turbidity currents, which moved silty and sandy material from the shelf margins of the Pindos basin down and onto the abyssal plain of the Pindos ocean, where – between successive debris flows - they became interbedded with limestones. The sand, silt, and mud comprising Flysch Transition Beds were derived from erosion of the uplifts created by thrust faulting and folding during closure of the Pindos basin (Degnan and Robertson, 1998).

This formation is marked by a wide variety of alternating lithologies, which markedly pronounces its bedded, stratified, layered appearance (Figure 20A). Limestone beds (typically ranging up to 50 cm in thickness) make up more than 50% of the formation. The limestones are interbedded with fissile red mudstones, jointed brown and beige sandstones, siltstones, fissile marls, and occasional chert layers. Some thin, fissile limestone beds have a glassy-sounding resonance when struck with a hammer.

Figure 20. Flysch Transition Beds.

A. Outcrop of folded limestone, with fracture-like features that may well be incipient spaced cleavage. Field notebook for scale.

B. The fold presented above, in A, is in the background. The foreground shows flat-lying, unfolded limestone. A small detachment separates these two outcrop domains. The detachment probably is marked by shale/mudstone interbeds in the formation.

C. Example of the typical geomorphic expression of Flysch Transition Beds in the area. Weathering and erosion transforms the bedrock into distinctive corrugated linear ridges. In the background is an immense expanse of Thick White Limestone Beds.

The internal stratigraphy of the Flysch Transition Beds lends itself to pervasive internal folding, for bedding surfaces penetrate the formation and there are plentiful incompetent interbeds that undoubtedly reduced sliding friction during bedding- plane slippage when folded (see Figure 20A). Folding within this formation is most evident in the limestone beds, because these beds crop out differentially and prominently. Not uncommonly the limestone beds in a given fold are seen to have tightened downward (during folding) to the point where no more shortening by folding was possible, whereupon the beds became detached from underlying incompetent lithologies, such as shales and mudstones, which may show no evidence of folding at all at *that* location (Figure 20B).

The landscape expression of Flysch Transition Beds is quite distinctive in the study area, in the form of mullion-shaped hillocks that have the appearance of flat-topped, linear corrugations, several hundreds of meters in length, 25 to 40 m or so in topographic relief. Narrow drainages straddle them on either side (Figure 20C). The upper surfaces of these corrugated ridges tend to have a flat, faceted appearance.

VII. GEOLOGIC MAPPING OF THE SANCTUARY

VII-A. Introduction

My geologic mapping of the study area was carried out during two weeks in the summer of 2004, two weeks in the summer of 2005, and four weeks (each) in the summers of 2007, 2008 and 2009. The scale of mapping was ~1:6000, using as base maps space-satellite imagery and topographic maps (contour interval 4 m). I recorded observations at ~800 stations, with attention given to identification of formation(s), rock type(s), geologic structures, and orientations of bedding, folds, and faults, and in certain instances joints and (rare) cleavage. I shot abundant digital photographs of the geology in order to assure a comprehensive descriptive record. Orientation and location data were recorded in an Excel file, and ArcMAP was used to fashion geological map products for GIS analysis and interpretation.

My geological map of the Sanctuary of Zeus study area is presented as Figure 21. In addition I created a "geostructural column" to portray the basic structural geologic relations within the Mt. Lykaion map area (Figure 22). The geostructure column, among other things, distinguishes relationships in the western two-thirds of the area ("west domain") and the eastern one-third of the area ("east domain"). The pivotal structural feature in the area overall is the Lykaion thrust.

Figure 21. Geologic map of the Sanctuary of Zeus, Mt. Lykaion.

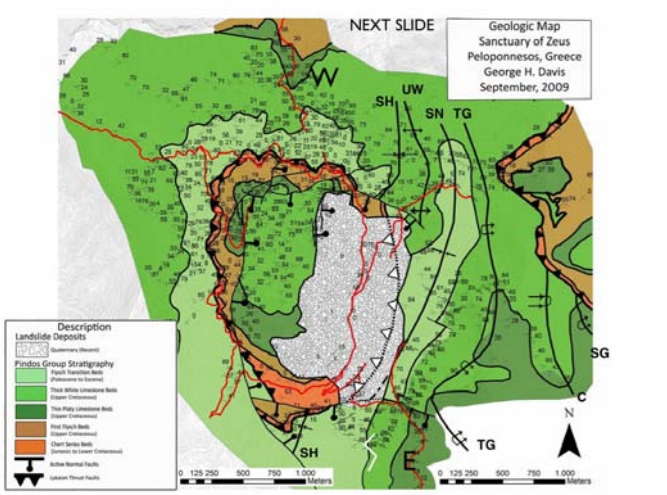

Mapping by George H. Davis, with field assistance from Tom Fenn, Randy Goosen, Phil Nickerson, and Karl Yares.

Figure 22. Schematic picture of structural geology of Mt. Lykaion study area.

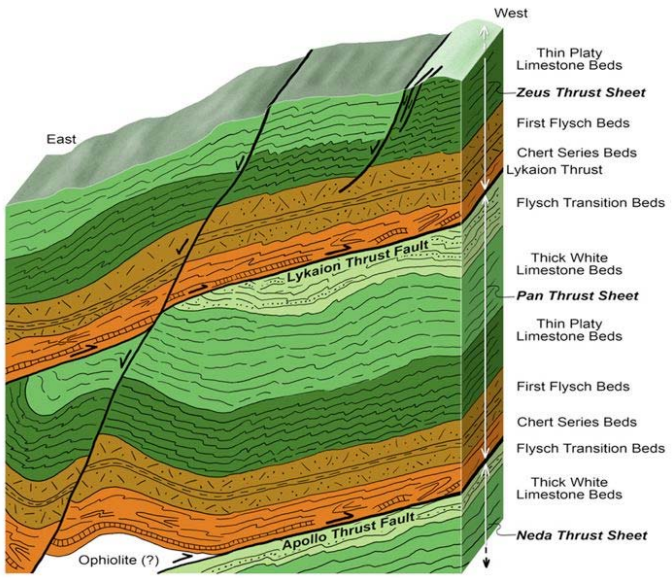

This 'geostructural column' diagrammatically summarizes the fundamental structural relations and properties derived from the geologic mapping. Note that two domains are specified, labeled "west" and "east."

VII-B. West Domain Faulting and Folding

VII-B1. Overall Structural Relationships.

The singularly distinctive geologic map pattern in the western two-thirds of the area expresses the presence of a roughly elliptical, closed-loop trace of a major subhorizontal thrust fault (see Figure 21), which I have named the *"Lykaion thrust fault."* Its expression in the landscape is pronounced (Figure 23). Immediately above the fault is an ascending stratigraphic succession of four of the five mappable formations, namely the Chert Series Beds, First Flysch Beds, Thin Platy Limestone Beds, and Thick White Limestone Beds, all in proper stratigraphic order (see Figure 23). Below the Lykaion thrust is Flysch Transition Beds resting on top of a descending stratigraphic succession of Thick White Limestone Beds, Thin Platy Limestone Beds, First Flysch Beds, and Chert Series Beds, again in proper stratigraphic order. The geological mapping reveals quite clearly a concentric elliptical pattern of the distribution of the Pindos Group formations (see Figure 23).

Figure 23. View of Sanctuary of Zeus from the north.

A. Photograph of Lykaion thrust fault and St. Eljah klippe, view to the south.

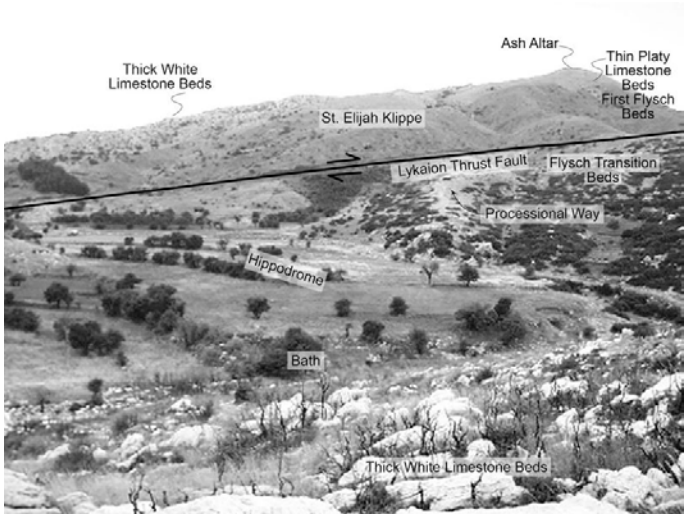

B. Annotated rendition, with identification of some of the rock formations, structures, and archaeological elements.

The Lykaion thrust fault, therefore, is a structure that marks a boundary between two thrust sheets of the Pindos stratigraphic formations. The upper sheet, exposed in the western two-thirds of the area, is a tectonic "klippe" (see Figure 23). It is composed of upper thrust sheet formations tectonically transported over lower thrust sheet formations that were once laterally removed, in all probability, by several kilometers or more. Subsequent to the thrust faulting, the upper thrust sheet rocks were partially removed, through erosion, to leave Mt. Lykaion as an isolated klippe (Figures 24). For reference I have named the klippe the "St. Elijah" klippe (after "Agios Elias," the mountaintop saint); the upper thrust sheet, the "Zeus

thrust sheet;" and the lower thrust sheet, the "Pan thrust sheet." At the base of the Pan thrust sheet is another thrust (see Figure 22), which I have named the "Apollo thrust fault," whose trace expression lies just outside of (west of) the Mt. Lykaion map area proper. (I believe that this thrust fault might pass close to the Temple of Apollo at Bassi). Its presence is quite clear, with Chert Series Beds (above) faulted upon Flysch Transition Beds (below). The thrust sheet beneath the Apollo thrust fault is here called the Neda thrust sheet.

Figure 24. View of the St. Elijah klippe from the west.

This is a view from the northwest side of Agios Elias. In the foreground is terrain underlain by limestone (Thick White Limestone Beds and Flysch Transition Beds), belonging to the Pan thrust sheet. The location of the Lykaion thrust is where the uppermost part of this limestone terrain gives way to smooth slopes lacking obvious bedrock. Above the thrust is the Zeus thrust sheet. Near the base of it are smooth slopes underlain by Chert Series Beds and First Flysch Beds. Thin Platy Limestone Beds can be seen in the distant background, at the top.

An imperfect bulls-eye distribution of Thin Platy Limestone Beds and Thick White Limestone Beds is evident at the top of Mt. Lykaion (see Figure 21). The complexity of the map pattern in this particular part of the area is due to moderate- to high-angle normal faulting of rocks within the Lykaion klippe. These faults juxtapose First Flysch Beds, Thin Platy Limestone Beds, and Thick White Limestone Beds in abrupt and angular, compartmentalized patterns. The nature and significance of this faulting will be described below in section VII-D.

VII-B2. Orientation of Lykaion Thrust, and the Thrust Sheets

The orientation of the Lykaion thrust fault underlying the St. Elijah klippe was determined through three-point methodology applied to the fault contact separating Chert Series Beds (above) and Flysch Transition Beds (below) (see Figures 21 and 22). The solution yielded a strike of N33°E and a dip of 10°SE. Thus this thrust fault within the west domain is very gently inclined, consistent with the observation that the apparent dip of the thrust in places is very close to horizontal (see Figures 23 and 24).

Within the Pan thrust sheet, and thus beneath the Lykaion thrust fault, the overall orientation of the stratigraphic formations seems best reflected in the stratigraphic contact between Flysch Transition Beds (above) and Thick White Limestone Beds (below) (see Figures 21 and 22). Three-point determination of this contact yielded a strike of N37°E and a dip of 5°SE. The orientation of the Lykaion thrust compares favorably with the orientation of the plane of best fit to the upper faceted surfaces of the corrugated landforms underlain by Flysch Transition Beds just beneath the thrust (see Figure 20C). In particular, three-point methodology applied to the tops of the corrugations resulted in a N22°E, 2°SE solution, which is an orientation essentially parallel to the attitude of the Lykaion thrust fault.

Within the St. Elijah klippe (*i.e.*, within the Zeus thrust sheet) the apparent overall macroscopic orientation of stratigraphic units appears best expressed in the map pattern of the base of the First Flysch Beds, where these beds are in contact with the top of the Chert Series Beds (see Figure 21). This lower contact of First Flysch Beds can be traced without interruption around the full extent of the northern and western flanks of the St. Elijah klippe. A three-point determination of the attitude of this contact reveals that it strikes N35ºE and dips 8ºSE. It is this orientation that is used as the basis for constructing the dip inclinations of the major stratigraphic units above the Lykaion thrust fault, as shown in Figure 22.

VII-B3. Analysis of Bedding Attitudes in the Pan Thrust Sheet

Further structural analysis was helpful in reconciling the overall gentle structural and stratigraphic orientations with the significant range of strike and dip variability within each of the mapped formations. Data were plotted stereographically using the *Rockware StereoStat* software

program developed and written by Stephen Ahlgren. The most revealing plots are contoured lower-hemisphere equal-area projections of all poles to bedding in the Pan versus Zeus thrust sheets (Figure 25). For bedding orientations measured in the Pan thrust sheet, the contour plots feature great-circle girdles along which two modes of pole concentrations are evident. We see this in the composite diagram (see Figure 25A), which shows contoured poles to bedding attitudes measured in Thin Platy Limestone Beds, Thick White Limestone Beds, and Flysch Transition Beds in the Hippodrome thrust sheet. The dominant modal concentration (I) reflects an average orientation of N20°E, 35°SE, and the subordinate modal concentration (II) reflects an average bedding orientation of N10°W, 40°SW.

Figure 25. Stereographic projections of poles to bedding, Pan plate and Zeus plate.

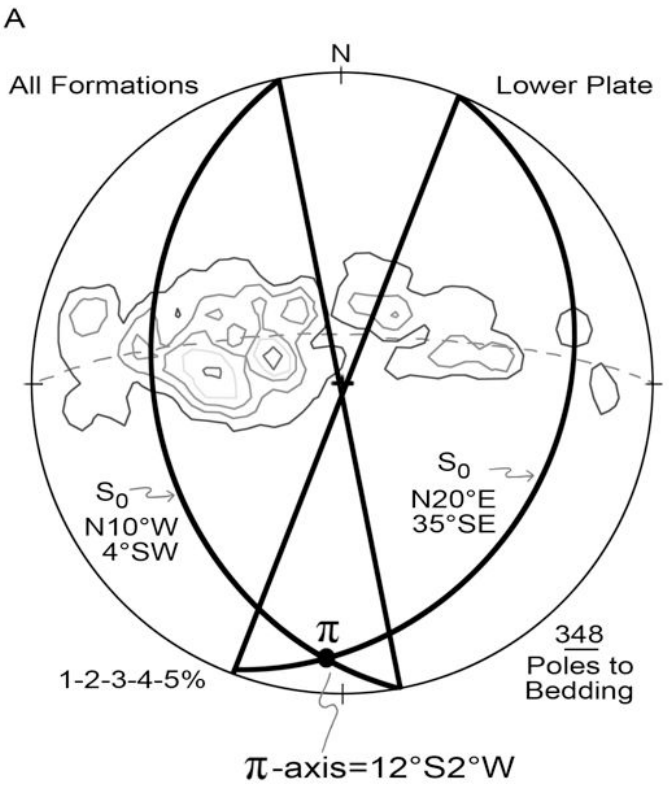

A. Lower-hemisphere equal-area stereographic projection of poles to bedding in the Pan thrust sheet in the West Domain of the map area. Contours are percentage of total data points falling within each 1% area of the net. The number of measurements are as follows: Thin Platy Limestone Beds, 18; Thick White Limestone Beds, 141; and Flysch Transition Beds, 179.

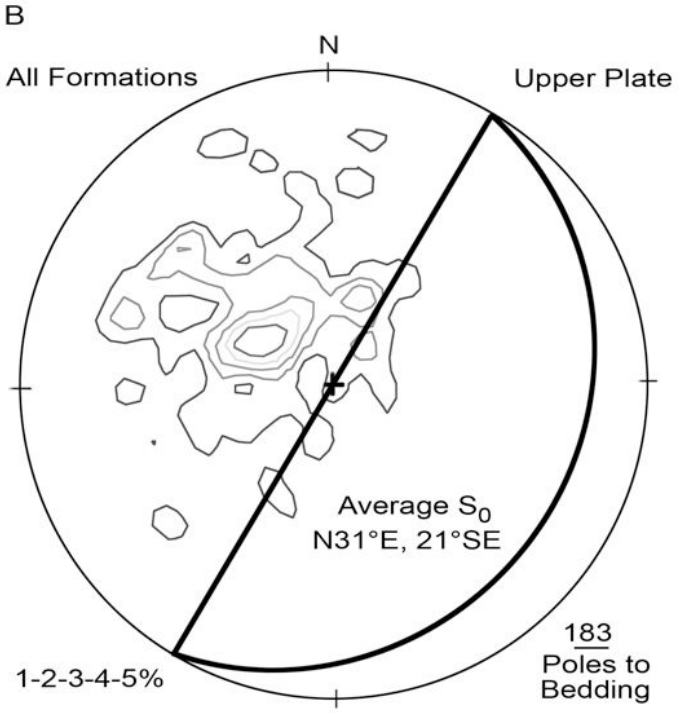

B. Lower-hemisphere equal-area stereographic projection of poles to bedding in the St. Elijah klippe. This is a composite plot for all measurements within the Chert Series Beds (31), First Flysch Beds (34), Thin Platy Limestone Beds (42), and Thick White Limestone Beds (62).

The dominant modal concentration for bedding strike in the Pan thrust sheet (*i.e.*, N20°E) departs approximately 15° counter-clockwise from the strike orientations determined through three-point methodology (N35°E, N33°E, and N37°E) for First Flysch Beds in the St. Elijah klippe, the Lykaion thrust fault, and the stratigraphic contact between Flysch Transition Beds and Thick White Limestone Beds in the Pan thrust sheet. The dip inclination reflected in the dominant modal concentration (*i.e.*, 35°SE) is slightly steeper than the dip determinations derived through three-point methodology for the dip of the thrust (*i.e.*, ~10º SE), and the mapped formations in the Zeus thrust sheet (ranging from ~8º to ~30ºSE) and in the Hippodrome sheet (~5ºSE). The subordinate modal concentration (N10°W, 40°SW; see Figure 25A) seems to reflect the average orientation of short limbs in the westward-verging asymmetrical folds within the Pan thrust-sheet formations. The girdle of points, overall (see Figure 25A), is a *p*-circle consistent with folding about a modal fold-axis orientation of 12°S, and a modal axial-surface

orientation of N-S, 90º. The combination of the analysis of map patterns and the stereographic projections reveals that the various Pan thrust sheet formations are not, together, folded into large anticlines and synclines. Instead, each formation has retained an overall tabular appearance and orientation, with the folds relatively small in size and embedded within each major stratigraphic unit. Thus the picture is one of disharmonic folding (see Figure 22).

VII-B4. Analysis of Bedding Attitudes in the Zeus Thrust Sheet

Figure 25B is a lower-hemisphere stereographic projection of all poles to bedding for measurements taken within the Zeus thrust sheet, in Chert Series Beds, First Flysch Beds, Thin Platy Limestone Beds, and Thick White Limestone Beds. No great-circle distribution of poles to bedding is evident, but instead there is a single modal concentration, reflecting a dominance of homoclinal inclination of bedding. The unimodal concentration coincides with an overall average strike and dip orientation of N31°E, 21°SE. The average strike orientation corresponds closely to the strike value determined by three-point methodology for the lower contact of the First Flysch Beds (N35°E) in the Zeus thrust sheet within the St. Elijah klippe, the strike of the Lykaion thrust fault (N33ºE), and the stratigraphic contact between Flysch Transition Beds and Thick White Limestone Beds (N37°E) in the Pan thrust sheet. However, the measured orientations of bedding dip tend to be steeper on average (*i.e.*, 21°SE) than the overall dip of First Flysch Beds in the St. Elijah klippe (8°SE), the dip of the Lykaion thrust fault (10°SE), and the dip of the stratigraphic contact between Flysch Transition Beds and Thick White Limestone in the Pan thrust sheet (5°SE).

Finer analysis of bedding orientations for each of the formations within the St. Elijah klippe integrate into what appears to be a steady, systematic counter-clockwise shift in average strike orientation, by formation, down-section through the St. Elijah-klippe stratigraphy toward the Lykaion thrust. The youngest formation is Thick White Limestone Beds, and the average orientation of bedding within this formation is N65°E, 30°SE. Stratigraphically beneath this formation in the St. Elijah klippe is the Thin Platy Limestone Beds, and its bedding attitude averages N40°E, 20°SE. Deeper still is First Flysch Beds, with an average bedding orientation of N20°E, 30°SE. For the Chert Series Beds, immediately above the Lykaion thrust fault, the average bedding orientation is N26°E, 23°SE.

The counter-clockwise shift in strike of bedding (progressively) downward in the St. Elijah klippe suggests that the thrust-shearing associated with tectonic transport of the Zeus thrust sheet had the effect of 'streamlining' bedding orientations, formation by formation, toward closer parallelism with the strike attitude of the Lykaion thrust fault. The N65°E average strike of the Thick White Limestone Beds, which is furthest above the Lykaion thrust, departs most significantly from the N33°E strike of Lykaion thrust fault.

VII-B5. Analysis of Outcrop-Scale Folds in the Thrust Sheets

Analysis of folds in Thin White Limestone Beds within the Pan thrust sheet was based upon field work, stereographic analysis (see Figure 25), examination of photographs of outcrop-scale folds for which measurements were taken, and study of notes of limb-dips of these folds, Folds within the unit are essentially symmetrical, with *'synthetic'* limbs (*i.e.*, dipping in the same direction as the Thin Platy Limestone Beds as whole) striking N5°E and dipping 35°SE, slightly more steeply than the overall formation. The stereographically determined modal axial plane orientation for these data is essentially north-south striking and vertical.

The stereographic features within the pole diagrams for bedding within the Thick White Limestone Beds and the Flysch Transition Beds reveal what can be seen in outcrop. The dominant folding is asymmetric intraformational folding marked by relatively long synthetic limbs dipping in the same direction (though more steeply) as the overall formation attitude, and by relatively short antithetic limbs dipping in the opposite direction to the overall inclinations of these formations. The average fold-axis orientation is identical for each of these formations. The stereographically determined modal fold axis orientation for each is 10° S2°E. The angle of fold-axis plunge (10°) is thus very close to the average dip (5°) for the formations viewed macroscopically, revealing that the fold hinges are not only contained within the formation but have axes that are coplanar with the overall attitude of the formation. There is also a close similarity in orientation between the dominant (synthetic) limb mode (I) seen stereographically for the Thick White Limestone Beds (N15°E, 35°SE), and that of the Flysch Transition

Beds (N12°E, 30°SE). Furthermore, there is a reasonably close correspondence in attitude between the secondary (antithetic) limb mode (II) for these same two formations (N19°W, 35°W for Thick White Limestone Beds; N9°W, 43°W for Flysch Transition Beds). Axial-surface orientations of the fold structures in all three of the formations are the same, namely NS-striking and dipping essentially vertically.

The physical manifestation of geometric measurements is a reasonably penetrative fold pattern marked by asymmetry. The asymmetry is one marked by a distinct westward fold vergence, which is consistent with tectonic transport by thrusting generally from east to west. This direction of transport is well documented regionally for the Pindos fold and thrust belt. Moreover, the fold-axis orientations (essentially due south) are consistent with an interpretation that here, within the sanctuary, the tectonic transport was truly from due east to due west. This interpretation is further confirmed by the presence of crystal-fiber lineations on shear surfaces seen in limestone outcrops in the Pan thrust sheet that show a preferred orientation essentially east-west. Furthermore, stereographic plotting of a number of hinges of outcrop-scale fold structures shows a preferred orientation of N-S, *i.e.*, at right angles to direction of tectonic transport.

In some ways the most interesting observation from fieldwork and fold analysis is that the various formations in the west domain within the Pan thrust sheet are not, together, folded into large anticlines and synclines. Instead, each formation has retained an overall tabular appearance and orientation, with the folds relatively small in size and sandwiched intraformationally within each major stratigraphic unit. Thus the picture is one of disharmonic folding (see Figure 19). It would appear that internal to each formation the fold attributes are driven by the standard controls for free folding: strength contrasts between mechanically stiffer and softer layers, and thicknesses of stiff layers. It would appear that the driving mechanism is layer-parallel (thrust) shearing. If this is true, the fold properties may be a guide to estimating shear strain magnitudes within each of the formations within which folding is penetrative. It is probable that the pervasive outcrop-scale folding largely represents layer-parallel shortening before the onset of major folding and thrusting.

VII-C. East Domain Faulting and Folding

VII-C1. Overall Structural Relations

The eastern third of the map area contains a system of major folds, and these reside in the Pan thrust sheet (see Figures 21 and 22). The folds are westward-overturned anticlines and synclines, which trend north-south and plunge at very low angles. Also in the east domain is another exposure of the Lykaion thrust fault, which dips ~25°E and places Chert Series Beds in the immediate hanging wall upon Thick White Limestone Beds on the immediate footwall (see Figure 21). The Chert Series Beds is generally poorly exposed here, not only because of the incompetence of the lithologies, but because the Chert Series Beds formation has been thinned and locally eliminated through thrust-related shearing.

The location of the exposure of the Lykaion thrust fault in the east domain stands out boldly, for the dark-colored hanging wall strata contrasts strikingly with the white footwall strata (Figure 26). Sandstones within the First Flysch Beds in close proximity to the Lykaion thrust fault are strongly fractured and faulted (Figure 27A). Some ancillary thrust surfaces stand out as distinctly smooth and planar (Figure 27B). Before erosion to create Mt. Lykaion as we see it today, the (Lykaion) thrust fault exposed along the eastern margin of the map area was co-extensive with the thrust fault surface beneath the St. Elijah klippe to the east.

Figure 26. East-view of Lykaion thrust fault, placing dark on light.

East-directed photograph of exposure of Lykaion thrust fault in the east domain of the map area. The thrust is "black on white." The white limestone outcrops in the foreground belong to the Thick White Limestone Beds formation within the Pan thrust sheet.

The dark outcrops at the summit belong to the Chert Series Beds and First Flysch Beds, and comprise a part of the Zeus thrust sheet.

Figure 27. Thrust fault damage within First Flysch Beds.

A. Photograph of faulted, fractured sandstone of the First Flysch Beds near the Lykaion thrust fault.

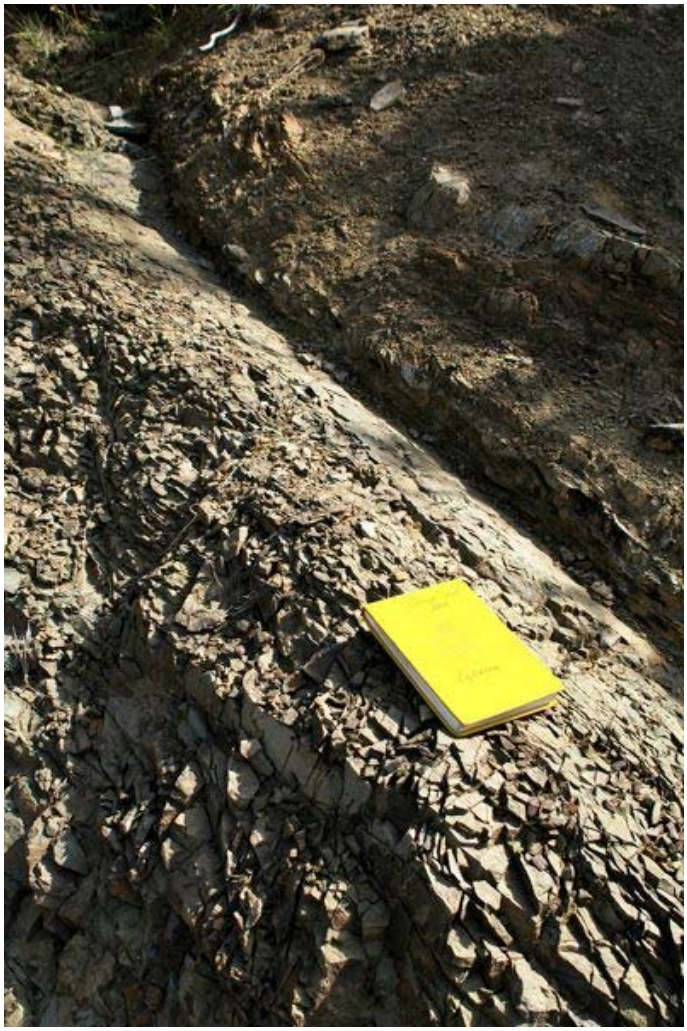

B. Photograph of a discrete fault surface within First Flysch Beds near the Lykaion thrust fault proper.

This thrust exposure represents a deeper level of thrust faulting than what is evident along the base of the St. St. Elijah klippe, because Flysch Transition Beds are missing. Chert Series Beds rests in fault contact on Thick White Limestone Beds. In contrast, along the base of the St. St. Elijah klippe, Chert Series Beds rests on Flysch Transition Beds (see Figure 21). This difference is consistent with the interpretation that the direction of thrusting was from east to west (Peter DeCelles, 2008, personal communication).

Macro-folding is the dominant structure in the east domain. The expressions of folds in the landscape are magnificent! There are six major fold structures (see Figure 21), named here (from west to east) the Sheep Herder's syncline (after permanent sheep station in south part of map area), the Upper Walnut anticline (after the village of "Ano Karyes"); the St. Nicholas syncline (after

"Agios Nikolaus"); the Three Gorges anticline (after "Tria Remmata"); the Cretea syncline (one limb of which projects to Cretea ridge), and the St. George anticline (after "Agios Georgios"). The southern part of the Upper Walnut anticline and much of the Sheep Herder's syncline are covered by extensive landslide deposits (see Figure 21). The St. Nicholas syncline is well exposed near a tiny chapel of the same name. Part of its expression is the strike ridge of Thick White Limestone Beds that trends north-south just east of the village of Ano Karyes (see Figure 21). The continuity of strike ridges within this fold is broken by east-west-trending compartmental faulting, which has produced right-lateral strike-slip separations of tens of meters (Figure 28; see also Figure 21).

Figure 28. Compartmental faulting evident along strike ridge.

North-directed view of strike ridge of Thick White Limestone Beds, which here define part of the overturned east limb of the St. Nickolas syncline. Note how "compartmental faults" at right angles to the strike ridge cause abrupt offset of the limestone bedrock. The shifts tend to be right lateral. The overall effect is obvious when comparing the location of the western boundary of the marker unit in the lower left corner of this photo, versus the location of this same horizon off in the distance. The village of Ano Karyes lies in the background; this, our home for the project. Also note that in the far distance (back right), the expression of rocks in the landscape reveal the location and orientation of the Lykaion thrust fault (also pictured in figure 26). The dark-weathering bedrock in back right is the Zeus thrust sheet. The light-weathering bedrock is the Pan thrust sheet.

Figure 29A captures the elegance of the Three Gorges anticline. The fold at this location is expressed in the weathered landscape expressions of the First Flysch Beds, Thin Platy Limestone Beds, and Thick White Limestone Beds, respectively. The ground distribution of First Flysch Beds is revealed by the dense cover of trees, accentuated because the trees were charred by intense wildfires during August, 2007. The brown sandstone lithologies that comprise the First Flysch Beds apparently favor soil development conducive to tree growth. Thin Platy Limestone Beds overlies the First Flysch Beds and is marked by its characteristic grassy and blocky landscape appearance (see Figure 29A). Stratigraphically above Thin Platy Limestone Beds are Thick White Limestone Beds. This formation is distinguished in the landscape by jutting, craggy outcrops topped by wiry bushes and trees, which at this location were significantly diminished by the wildfires (see Figure 29A). Thus, the landscape expressions of these three distinctive formations 'track out' the form of the overturned anticline!

Figure 29. Three Gorges anticline.

A. The form of the Three Gorges anticline can in places be seen in the landscape expression of bedrock formations. The core of the anticline is defined by the shape of the woods, which selectively grow on First Flysch Beds. The outer arc of the fold is defined by the white-weathered bold outcrop expression of Thick White Limestone Beds. In between is the anticlinal arch defined by grasslands and scrub underlain by Thin Platy Limestone Beds. The relationships are particularly graphic, because the woods are charred, burned by the fires of August, 2007.

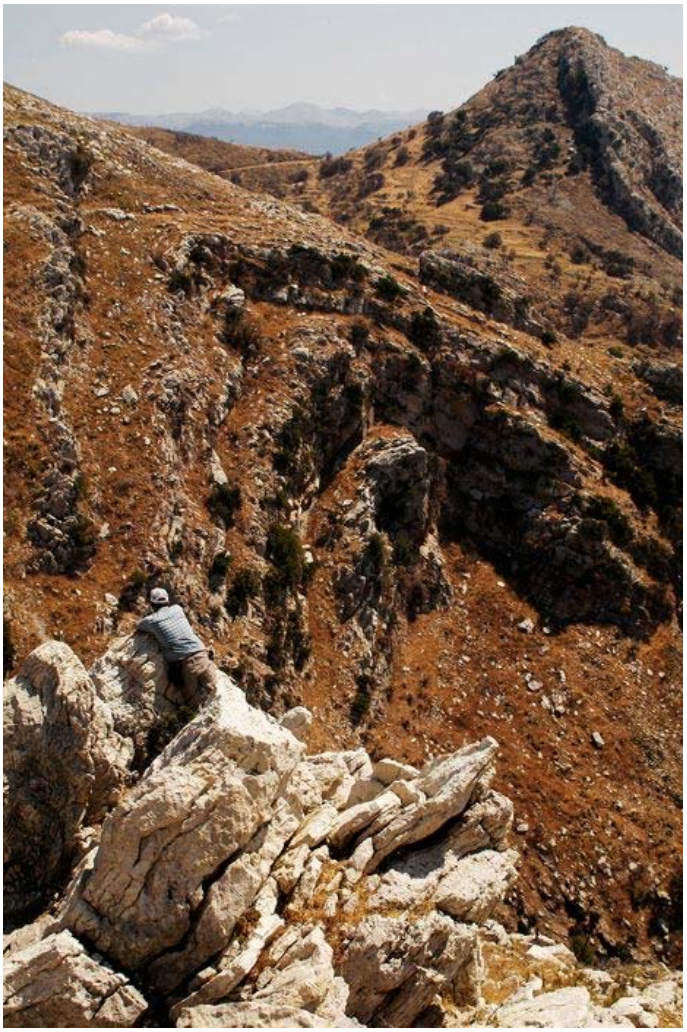

B. Photograph of Three Gorges anticline (middle ground). On the far right (upper right corner) is a resistant rib of limestone which represents the overturned eastern limb of the Cretea syncline. The rock spire that is held up by this limestone rib is known as Agios Georgios, for a chapel of that name is located at its very top. In left foreground, Phil Nickerson looks down into the Three Gorges drainage.

The Three Gorges anticline tends to be overturned westward (see Figures 21 and 29), though northward it becomes more upright (Figure 29B). To the east of it is the St. George syncline, which is overturned westward. The east limb of this syncline is also the west limb of the overturned Cretea syncline. The east limb of this syncline forms the steep rib of limestone that supports the hill-spire on top of which is located a chapel of St. George ("Agios Georgios") (see Figure 29B), which is located near the hinge of the overturned St. George anticline. One particular profile view of the Cretea syncline is especially dazzling (Figure 30), displaying a nearly isoclinal form expressed by limestones of the Thin Platy Limestone Beds and Thick White Limestone Beds formations. The room problem created during tight synclinal folding apparently created an out-of-the-syncline flow, accommodated by flexural-slip displacements and bedding-parallel faulting. Evidence for this is expressed in a particularly noteworthy profile view of the Three Gorges anticline (Figure 31). The lower part of this fold profile is a perfect upright, symmetrical anticline. In contrast, the upper part of this fold profile displays pronounced (westward) overturned to recumbent folding (see Figure 31). The overall effect is one of disharmonic folding. A likely explanation for the pronounced overturning and disharmony is out-of-the-syncline flow, emanating from the Cretea syncline. To the east of the Cretea is the St. George anticline, which is profoundly overturned westward (Figure 32).

Figure 30. Exquisite landscape expresion of Cretea syncline.

South-directed photograph of nearly isoclinal fold expression of the Cretea syncline. The limestone bedrock includes both Thin Platy Limestone Beds and Thick White Limestone Beds.

Figure 31. Disharmonic folding within Three Gorges anticline.

Nearly normal-profile expression of the Three Gorges anticline. View is northward. This is a beautiful example of disharmonic folding within Thick White Limestone Beds. The lower part of the fold is upright; the upper part of the fold is profoundly overturned westward.

Figure 32. Overturned limb of St. George anticline.

North-directed photo showing overturned nature of St. George anticline. Rocks belong primarily to Thick White Limestone Beds.

VII-C2. Orientation Analysis

As mentioned above, there is a prominent exposure of the Lykaion thrust fault in the eastern part of the study area (see Figures 21, 26, and 28). It strikes essentially N-S, and dips gently (~20° - 30°) to the east. The dip inclination is steeper than that part of the thrust that defines the base of the St. Elijah klippe on Agios Elios.

Bedding orientations in the Pan thrust sheet in the eastern third of the area are presented stereographically in Figure 33A. The poles to bedding define a great circle distribution reflecting systematic folding of the strata in the east domain. Fold hinges trend 352° and, on average, are absolutely horizontal. This span of orientation data in the eastern domain conforms nicely to that of all bedding orientation data collected throughout the Pan thrust sheet (Figure 33B): namely a great circle distribution conforming to an average fold-axis orientation of 10°S 5°W.

Figure 33. Stereographic projections in Pan thrust sheet.

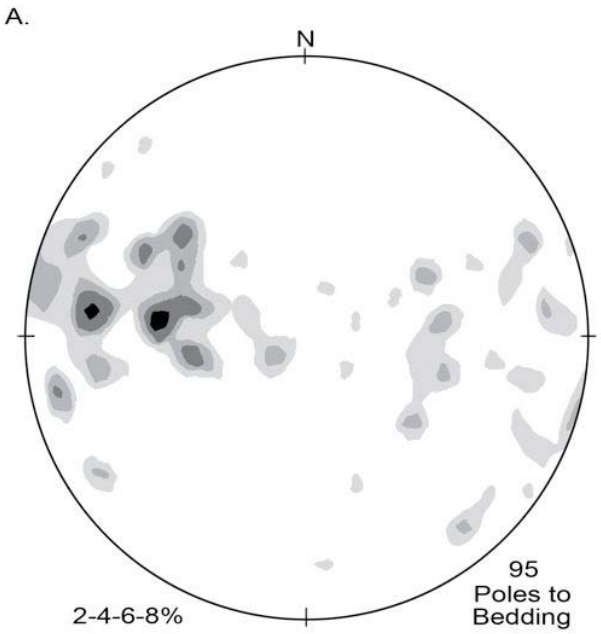

Contours are percentage of total data points falling within each 1% area of the net.

A. 95 poles to bedding in the eastern domain of the Pan thrust sheet.

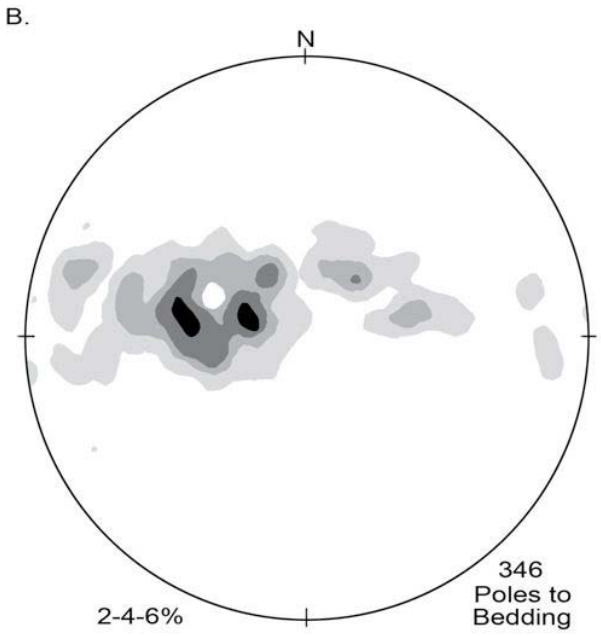

B. 346 poles to bedding throughout the Pan thrust sheet.

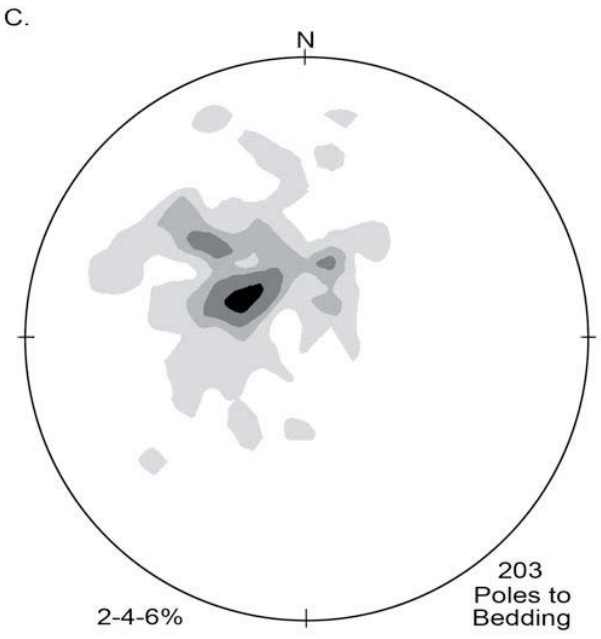

C. 203 poles to bedding throughout the Zeus thrust sheet. See text for explanation.

Map relationships and bedding data reveal that westward overturning is most pronounced in the three easternmost folds, *i.e.*, the uppermost part of the Three Gorges anticline, the Cretea syncline, and the St. George anticline (see Figure 21). The westernmost two folds (*i.e.*, the St. Nicholas syncline and the Upper Walnut anticline) are asymmetrical westward to upright, and for the most part NOT overturned. In fact the Upper Walnut anticline and Sheep Herder's syncline, which are the most upright, gentle, and ill-defined of the fold structures, together create part of the structural transition between the folded nature of strata in the east domain and the more homoclinal nature of strata in the west domain (see Figure 21). Additional geological mapping is required to pin down the traces and exact geometries of these folds within the northern part of the map area.

The great-circle distributions of bedding data for the Pan thrust sheet (see Figures 33A, B) contrasts sharply with the basic homoclinal attitude of bedding, overall, in the Zeus thrust sheet (Figure 33C). Average orientation of bedding within the Zeus thrust sheet is N35°E, 20° SE.

In the east domain of the Pan thrust sheet, the axial surfaces of the major folds (Sheep Herder's syncline, Upper Walnut anticline, St. Nicholas syncline, Three Gorges anticline, Cretea syncline, and St. George anticline) steadily strike ~N10°E. However, dips of axial surfaces within this fold system steadily decrease from near-vertical for the Sheep Herder's syncline and Upper Walnut anticline (on the west) to ~50°E for the St. George anticline (on the east).

VII-D. Active Faulting

VII-D1. Scree Bands as Guides to Faulting

My discovery of active normal faulting in part grew out of puzzlement over peculiar screen bands (composed of limestone blocks) in the area of the upper sanctuary, a good example of which is shown in Figure 34. There are a number of places where these linear swaths and bands of scree occur. They are up to ~12 m in breadth and ~50 m in uninterrupted trace length. Individual limestone blocks show faces that are typically square or rectangular, and the blocks most commonly range in size from fist to bread box. It is obvious there is a 'fine fraction' of rock in some of the bands as well, composed of fragments of mudstone and marl, in the form of small chips.

Figure 34. Scree band near base of ash altar summit.

The scree is exclusively limestone blocks from the Thin Platy Limestone Beds formation. Phil Nickerson is negotiating the pile. The scree band marks the trace of an active normal fault.

Scree or talus normally accumulates at the base of a cliff of broken but resistant rock representing the accumulation of rock falls from the over-steepened face. What makes these scree bands peculiar is that there are no cliffs. The scree bands simply occur mid-slope on a hill, or perhaps at or near the base of a hill. In many cases it is apparent that the scree bands coincide with a slight smooth 'step' in the topography, on the order of a half meter to several meters (Figure 35). Almost all of the scree bands are derived from Thin Platy Limestone Beds, although there are places where the limestone scree was derived from Thick White Limestone Beds. The progressive development of the scree bands seems straightforward. Episodes of faulting create scarps in the landscape, exposing in places footwall bedrock of Thin Platy Limestone Beds. The fault scarps that develop are initially very steep (greater than ~70º). However, because bedding in this limestone is platy and excessively fractured (Figure 36), weathering and erosion causes the footwall scarps to collapse. They simply cannot hold up to the constant 'tug' of gravity. As a consequence, the scree derived from footwall collapse progressively buries the fault surface, and the fault scarp becomes reduced in height and slope angle.

Figure 35. "Steps" in hillside, caused by active faulting.

When the scree bands are viewed from just the right vantage, they are seen to coincide with 'steps' or breaks in topography, in the form of subdued rounded scarps, abrupt changes in elevation, and differences in slope angles above and below. This photograph was taken on the flank of the ash altar hill, *i.e.*, Agios Elios.

Figure 36. Outcrop expression of weakness of Thin Platy Limestone Beds along fault zones.

The unit breaks up into blocks ~15 cm x 15 cm, reflecting the fact that bedding thickness is essentially the same as fracture spacing. This is a particularly appropriate example of the lack of cohesion of this formation, for this outcrop is immediately adjacent to an active fault zone.

Thus one of the significant discoveries resulting from my geological mapping of the Mt. Lykaion Sanctuary of Zeus was recognition of active normal faulting. The faulting is especially concentrated and/or especially obvious near the crest of Mt. Lykaion in the Zeus thrust sheet,

where several formations of the Lykaion klippe are cut and displaced (Figure 37). The mapping of these faults proved to be relatively straightforward, not only because the linear scree bands define the fault trace expressions, but also because beyond the "tips" of the scree swaths it was possible to continue to map active faults on the basis of abrupt truncation and juxtaposition of stratigraphic formations.

Figure 37. Geologic map of active faults in the St. Elijah klippe

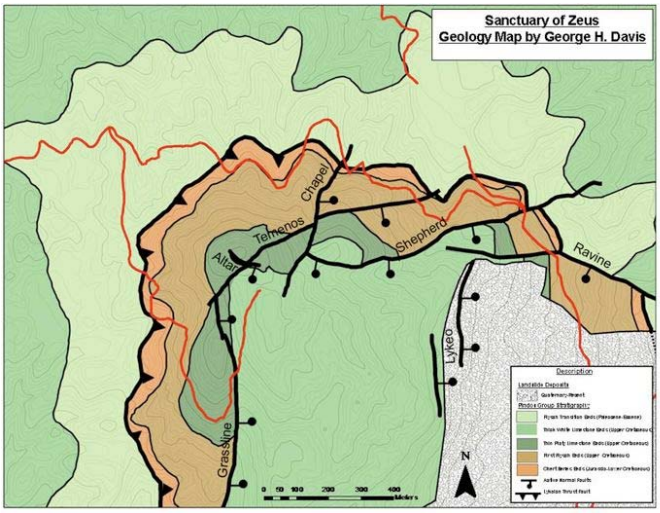

Names of faults are shown. Mapping assisted by Phillip Nickerson.

VII-D2. Active Faulting within the St. Elijah Klippe

The map pattern of active normal faults in the St. Elijah klippe is presented in Figure 37. I have named these for convenience of reference. From west to east across the summit of the sanctuary they are the Grassline fault, the Temenos fault, the Ash Altar fault, the Chapel fault, the Shepherd fault, and the Ravine fault (see Figure 37).

The Grassline fault is major active normal fault with a trace length of at least 2.5 km (see Figure 37). It strikes NS, dips ~60º-70ºE, and is marked by down-to-the-east offset. Near the summit it passes along a narrow grassy strip (Figure 38), interpreted by David Romano as a possible site of an early stadium in the upper sanctuary. At the north end of the Grassy fault, Thin Platy Limestone Beds on the west (footwall) are faulted against Thick White Limestone Beds on the east (hanging wall) (see Figure 37). Stratigraphic throw is ~65 m. To the south the Grassy fault is marked by ever-increasing stratigraphic throw, up to at least ~150 m (see Figure 21). Because elevation drops along it from north to south, exposures of the Grassy fault southward reveal deeper and deeper structural levels. The Lykaion thrust is clearly cut and displaced by the Grassy fault (see Figure 21).

Figure 38. Landscape expressions of Grassline fault.

South-directed view of Grassline fault. Photograph taken from near the top of Agios Elias. The green swath represents an area where alluvium has accumulated, creating a cover of the bedrock. The fault itself is on the western (right) side of the grassy swath, at the base of the ridge. Bedrock underlying this ridge is Thin Platy Limestone Beds. Bedrock exposed on the east side of the grassy swath is Thick White Limestone Beds. Near the intersection of the fault trace and the road the location of the Grassline fault is tightly constrained, for Thick White Limestone Beds (white outcrops) are in direct contact with Thin Platy Limestone Beds.

The Temenos fault is an active normal fault with a trace length of ~700 m (see Figure 37). It strikes N40ºE, dips ~60ºSE. The western part of the fault trace is marked by a broad, thick accumulation of limestone scree (Figure 39A). It can be followed eastward right along the southern flank of the ash altar summit, and just west of the northern boundary of the temenos (Figure 39B). The SE block (hanging wall) of this fault has dropped relative to the NW (footwall block), as evidenced by the various juxtapositions of stratigraphic formations along the fault trace (see Figure 37). Both on the western and northern flanks of the St. Elijah klippe, this fault separates Thin Platy Limestone Beds of the hanging wall from First Flysch Beds of the footwall. Across the summit of the klippe, Thick White Limestone Beds (hanging wall) are dropped down relative to Thin Platy Limestone Beds (footwall). Stratigraphic throw is ~75 m. If this fault cuts and displaces the Lykaion thrust, as we expect it does, the offset is so small that it is unrecognizable; the fault

may tip out before reaching the trace of the Lykaion thrust.

Figure 39. Landscape expression of Temenos fault

A. North-directed photograph of the scree band marking the trace of the Temenos fault. The ash altar of the Sanctuary of Zeus is at the very summit at the top of the mountain, right background.

B. Northeast-directed photograph of the continuation of the Temenos fault. Ash altar hill in background. Scree band running parallel to the flank of the hill is the Temenos fault. The actual temenos is the flat area in the middle ground, now being used at times as a parking area. The scree band running from the top of the ash altar hill and at nearly right angles to the Temenos fault is the Altar fault, another active normal fault.

The Altar fault is a northwest-striking, southwest-dipping active normal fault which passes ~10 m west of the ash altar (see Figure 37). Its trace length is only ~30 m, and its displacement appears to be no more than 10 m. The Altar fault appears to cut and displace the Temenos fault, producing a right-lateral separation (see Figure 39B). The presence of an active normal fault so close to the ash altar heightens the sense of the 'powerful' nature of the sanctuary. In the summer of 2009 I initiated paleoseismic trenching into a colluvial wedge of limestone-block scree along the trace of the Altar fault. Slickenlined blocks were found to be abundant, creating in my mind the expectation that the fault surface itself will be penetrated during the 2010 field season of trenching.

The Chapel fault strikes N10ºE, is inferred to dip easterly, and has a short trace length of less than 0.5 km (see Figure 37). Near the summit of the upper sanctuary, the Chapel fault separates Thick White Limestone Beds on the east (hanging wall) from Thin White Platy Limestone Beds on the west (footwall). Stratigraphic throw is ~25m. Its trace can be followed north of the Temenos fault. No offset of the Lykaion thrust by the Chapel fault is discernable.

The Shepherd fault (see Figure 37) is a conspicuous normal fault associated in places with a profound linear accumulation of scree (Figure 40). The Shepherd fault strikes N75ºE, dips steeply to the southeast, and has a trace length of ~1.0 km. The hanging wall of this fault throughout most of its trace is composed of Thick White Limestone Beds. Footwall rock, from west to east along the fault trace, progresses down-structure through the Zeus thrust sheet, crossing Thick White Limestone Beds, Thin Platy Limestone Beds, First Flysch Beds, and Chert Series Beds to the Lykaion thrust fault, which it cuts and displaces. From there it cuts downward into the Pan thrust sheet, offsetting Flysch Transition Beds by as much as ~50m. The Shepherd fault is so named because of fault damage to a shepherd's hut and the burial of a shepherd's wall and/or hut by the scree.

Figure 40. Disturbance of Shepherd's wall by active faulting.

North-northwest-directed view of the Shepherd fault. The Shepherd fault runs along the base of a ridge of Thick White Limestone Beds. The volume of limestone scree is immense. Note that the Shepherd's wall runs directly toward the band of scree and appears to disappear. In the right background a part of a built structure is evident within, and covered by, the scree.

The Ravine fault branches eastward from near the midpoint of the Shepherd's fault (see Figure 37). It strikes west-northwest and dips southwest. It conspicuously cut and displaces the Lykaion thrust fault, producing a right-lateral separation of ~225 m (see Figures 21 and 37). Figure 41 is a west-northwest directed view of the Ravine fault at a location where hanging-wall First Flysch Beds of the Zeus thrust sheet are juxtaposed against Flysch Transition Beds and Thick White Limestone Beds in the footwall (which is the Pan thrust sheet). Stratigraphic throw is as great as ~500 m.

Figure 41. Ravine fault puts First Flysch Beds against Flysch Transition Beds.

West-northwest-directed photograph of the Ravine fault. The trace of the fault separates grassy ground on the left (south) from white limestone outcrops on the right (north). The fault dips left (*i.e.* southwest) at a moderately steep angle (~60º). The limestone outcrops are Flysch Transition Beds of the Pan thrust sheet, and represent the footwall of the active normal fault. Note that the grassy ground contains outcrops of brown sandstone, which is First Flysch Beds of the Zeus thrust sheet, representing the hanging wall of the fault. Goat herd for scale.

VII-D3. Active Faulting Bordering St. Elijah Klippe on East

The largest of the active normal faults shape the upper reaches of the eastern margin of Mt. Lykaion, where there are at least two majors north-south-striking, east-dipping normal faults (see Figures 21 and 37). The zone, which I call the Lykeo fault zone has a trace length of at least 1.0 km. The faulting is expressed clearly in a systematic eastward down stepping of the Mt. Lykaion mountain-top surface (Figure 42A). There are at least two subhorizontal structural terraces (featuring both bedrock and scree), which have stepped downward by the faulting. These terraces contain large limestone blocks that have been shaken down from above but managed not to roll off the terrace(s) to the east (Figure 42B).

Figure 42. Landscape expression of the Lykios (active) fault zone.

A. South-directed photograph of the steep eastern flank of the upper reaches of the Sanctuary of Mt. Lykaion. Bedrock is entirely Thick White Limestone Beds of the Zeus thrust sheet. The abundance of scree, and the number of precariously balanced limestone blocks, testify to the active nature of this faulting. The active faults appear to be dipping ~60ºE, given the inclination of the scarp whose profile is so evident. At the base of the uppermost fault/scree slope there is a broad, flat structural terrace. This appears to be the first step down from the eastern edge of the summit plateau of Mt. Lykaion, and reveals a net fault displacement for this part of the zone of at least ~40m.

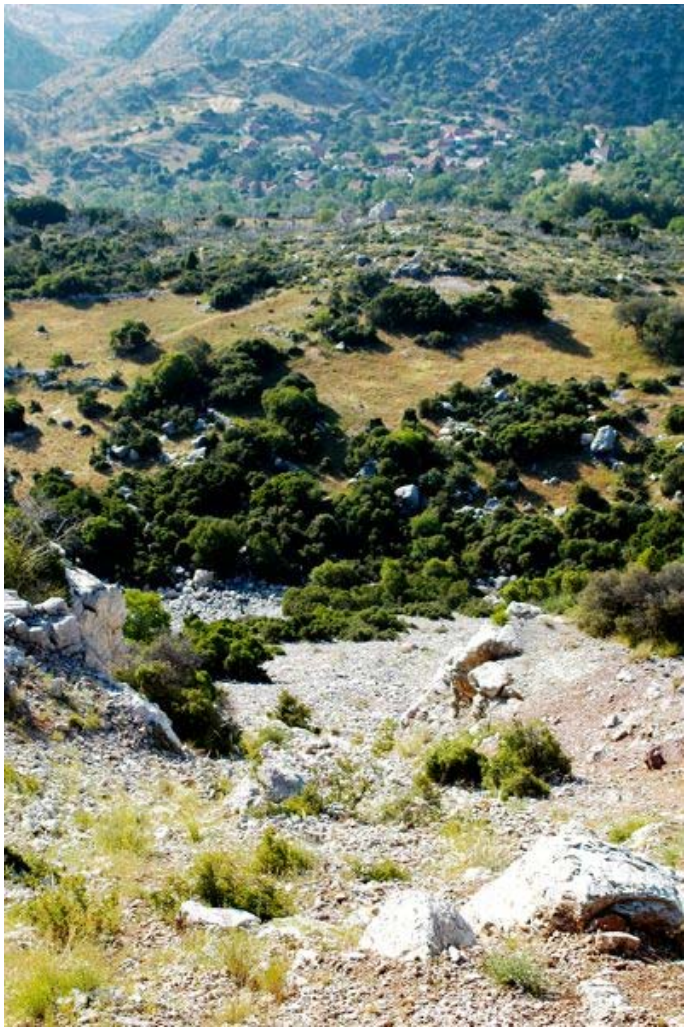

B. Southeast-directed photograph from the eastern edge of the structural terrace noted above. From this vantage a second structural terrace can be seen, which is largely tree-covered. It is represents the tsecond step created by displacements within the Precipice fault system. The village of Ano Karyes is directly downslope, and as noted earlier in the text the village has been built on landslide deposits.

The escarpments along the Lykeo fault zone are tall, at least 40m. Though the underlying bedrock (Thick White Limestone Beds) is covered largely by limestone scree on the terraces and the lower reaches of the escarpments (Figure 43A), there is well-exposed bedrock in the upper portions of the headwalls. Notwithstanding, major bedrock outcrops appear from place to place to have shifted out of original positions and orientations, and some are precariously balanced (Figure 43B). The bedrock occupying the escarpments is unstable, because of steepness and strong internal fracturing. Evidence of rock falls is conspicuous.

Figure 43. Scree deposits and rock falls along Lykios fault zone.

A. Photograph of screen cones descending downward from a combination of limestone bedrock and cohesive landslide deposits of limestone.

B. Large precariously balanced blocks of limestone are perched upon these oversteepened slopes.

The characteristics of this major active normal-fault zone conform nicely to descriptions of active faulting in Greece where limestone is the dominant country rock (Stewart and Hancock, 1988; Goldworthy, Jackson, and Haines, 1992; and Goldworthy and Jackson, 2000, 2001).

VIII. GEOARCHAEOLOGY OF MT. LYKAION SANCTUARY

VIII-A. Concept of a Geoarchaeological Column

How are the archaeological elements of the Sanctuary of Zeus generally related to the geology? To this end I have constructed what I call a *"geoarchaeological column,"* which here displays the positioning of the Sanctuary of Zeus archaeological elements in relation to rock formations, stratigraphic contacts, geologic structures, and bedding orientation(s) (Figure 44). The companion illustration (Figure 45) is my *"geoarchaeological map,"* which displays the placement of the archaeological elements on a simplified version of the geological base map. Explicit in the geoarchaeological column is the thrust-fault repetition of stratigraphic formations, and thus the distinction of the Lykaion thrust sheet (above) and the Hippodrome thrust sheet (below). Affixed to the geoarchaeological column are the geologic positions of each of the archaeological elements.

Figure 44. Geoarchaeological column.

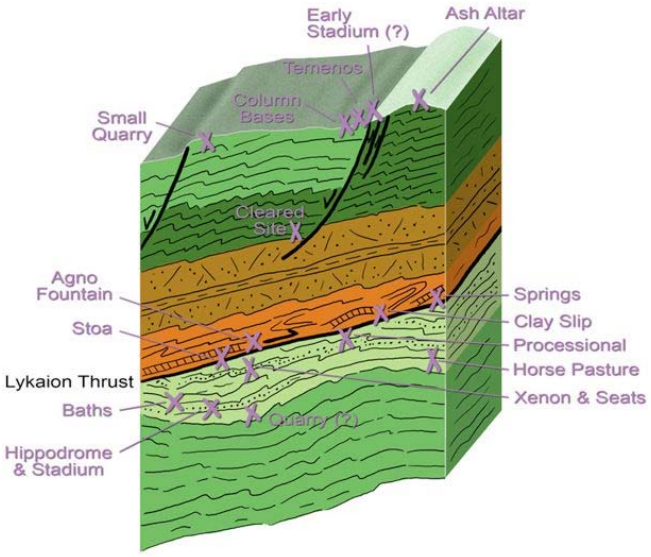

"Geoarchaeological column" showing the locations of the archaeological elements with respect to stratigraphy and structure. See text for details.

Figure 45. Geoarchaeological map.

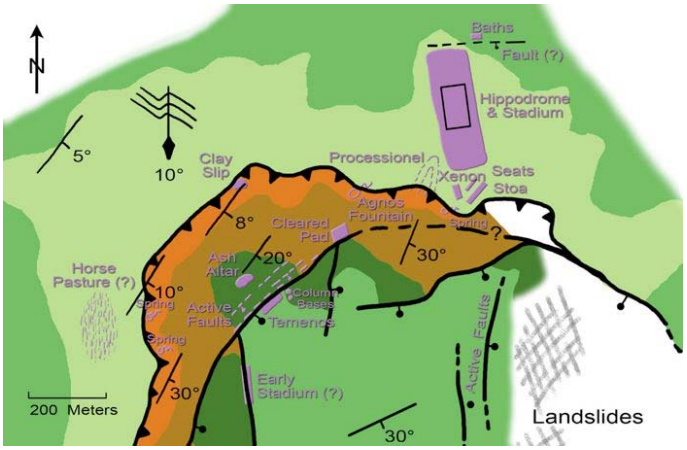

"Geoarchaeological map" showing the locations and (in some cases the) shapes of the archaeological elements with respect to the mapped geology. See text for details.

VIII-B. Archaeological Elements in the Lower Part of the Sanctuary

The archaeological elements of the lower part of the Sanctuary of Zeus reside in the uppermost part of the Pan thrust sheet. They are found exclusively in association with Transitional Flysch Beds and the Lykaion thrust fault proper. The major features are the hippodrome, stadium, bath, processional way, stoa, xenon, seating, and springs (see Figures 44 and 45).

The hippodrome, stadium, and bath occur within a flat expanse of landscape that coincides closely with the stratigraphic contact between Thick White Limestone Beds (below) and Flysch Transition Beds (above). The contact at this location is very gently dipping, nearly horizontal. The hippodrome surface is buried beneath a colluvial cover (no more than several meters thick), which is composed of sand and silt derived from weathering and erosion of the flank of Mt. Lykaion. It is likely that such a soft mantle of colluvium had developed in this flat expanse well before human occupation, and that the combination of the flatness and soil was a 'natural' for selecting this site for a hippodrome and stadium. The stone blocks of the bath complex are exclusively limestone from the Thick White Limestone Beds. The source and pathway of water that fed the baths is not yet clear, and is currently under study.

The processional way is a ridge that rises gently toward Mt. Lykaion from the southwestern corner of the hippodrome (see Figures 44 and 45). It appears to have been a pathway up the mountain. Underlying bedrock is Flysch Transition Beds. The ridge itself is one of the geomorphic corrugations so typical of weathering and erosion of Flysch Transition Beds.

The stoa, xenon, and seating lies just beneath the trace of the Lykaion thrust fault, in the uppermost part of the Pan thrust sheet (see Figures 44 and 45). All of these structures are built of limestone from the Thick White Limestone Beds. The foundation for these structures varies, in places Flysch Transition Beds bedrock, in other places colluvium. The stoa is closest to the trace of the thrust. Its foundation is locally anchored in limestone bedrock. Immediately above is the thrust and highly sheared Chert Series Beds of the Zeus thrust sheet. The sheared, faulted, crushed bedrock could have been easily 'swept' aside as needed during construction of the upper parts of the stoa.

Springs occur in the lower sanctuary, as well as along the western base of the St. Elijah klippe. Not unexpectedly, they emerge from the fault zone, where sheared Chert Series Beds creates a largely impermeable barrier to downward flow of groundwater within the Lykaion klippe. The remains of fountain houses and statues (*e.g.*, statue bases) are made exclusively from limestone from the Thick White Limestone Beds.

VIII-C. Archaeological Elements in the Upper Part of the Sanctuary

The archaeological elements of the upper part of the Sanctuary of Zeus are found at the very top of the St. Elijah klippe. The major features are a stadium (?), temenos, and ash altar. These are portrayed at the top of the geoarchaeological column and geoarchaeological map (see Figures 44 and 45). Each of these is located either in the Thin Platy Limestone Beds or Thick White Limestone Beds. Furthermore, these elements are arranged in a small, local area marked by active normal faulting.

The soft level grassy patch (~100 m X 15 m) along the trace of the Grassline fault near the top of the mountain may have been the site of a very ancient stadium in the upper sanctuary area (David Romano, personal communication, 2004). Fracturing and crushing of bedrock along this fault zone undoubtedly contributed to deeper weathering and erosion along this stretch, and the development of this grassy topographic depression.

The temenos also occupies a flat patch of ground (~60m NE/SW and ~20m NW/SE), and is located on the

shoulder of the very summit of Mt. Lykaion (see Figures 44 and 45). As has been noted, Its northwestern margin is close to the trace of the Temenos active normal fault. The flatness of the temenos fundamentally reflects the presence of a bedrock-supported structural terrace where bedding attitudes are horizontal to very gently dipping. The bedrock exposed from place to place within the temenos appears to be the thin-bedded stratigraphic transition between Thick White Limestone Beds (above) and Thin Platy Limestone Beds (below), composed of alternating layers of limestone and mudstone. The easy splitting property of this bedded interval must have been the main control for the weathering and erosion that, in this case, created a kind of natural pavement.

Bedrock supporting the summit of Mt. Lykaion at the site of the ash altar is Thin Platy Limestone Beds (see Figures 44 and 45), and its poor exposure reflects the ease with which the highly jointed, thin-bedded limestone becomes weathered and eroded. The smooth, colluvium-coated summit creates a soft and smooth form on the top of which the ash altar was created. The scree bands on the side of the ash altar hill are almost certainly the traces of active faults, such as the Altar fault.

IX. CONCLUSIONS

This contribution presents the stratigraphy and structural geology of the Sanctuary of Zeus at Mt. Lykaion in a way that is connected with the regional tectonic history and the active contemporary tectonics of the Peloponessos. The geological factors and conditions of the Sanctuary contributed to Mt. Lykaion arising as a pan-Arcadian and pan-Hellenic sanctuary. The geoarchaeological specifics are emerging from still-ongoing interdisciplinary field and laboratory activities central to the Mt. Lykaion Excavation and Survey Project. Already it is revealing how geological and tectonic factors relate to historical, political, economic, geographic, religious, and cultural dimensions of the Sanctuary of Zeus, Mt. Lykaion.

Acknowledgements

I am very grateful to David Romano and Mary Voyatzis for their inviting me to participate in the Mt. Lykaion Survey and Excavation; and for their leadership in assuring that investigations of the Sanctuary of Zeus would be profoundly interdisciplinary. I have benefited from their fund-raising efforts, which provided travel and logistical support for students including students who assisted me in the field. Funding from Exxon Mobil helped defray some of my operational expenses in Greece during the summer of 2008.

I am indebted to Andrew Insua for his specific technical guidance in helping me to establish a GIS-based data framework for my geological investigations. Randy Goosen carried out the initial steps in transforming hard copies of maps, and spreadsheets of data into an ARC-MAP system in the midst of the 2007 field season, when she served as my assistant both for field work and computer support. Meridith Reifsneider expertly enhanced and streamlined my ARC-MAP data bases and files during 2008 and 2009. Stephen Ahlgren gave me complementary use of the stereographic projection software (*StereoStat*) he developed.

I want particularly to thank Tom Fenn, who was my field assistant during two two-week stints of geological mapping, in the summers of 2004 and 2005. We worked together at the very start of the project, and his observations and inputs were particularly useful as we attempted to make sense of the stratigraphy and begin to trace the geological contacts. In addition, I want to thank Phil Nickerson, who was my field assistant for a 4-week stint of fieldwork in the summer of 2008; and Karl Yares, who assisted me for 4 weeks in the summer of 2009.

This work would not have been possible without the overall and sustained support of the Anastasia Panagiotopoulou, who at the time of initiation of the project was the Ephor in charge of the 5th Ephoreia in Sparta, and Michalis Petropoulos, Ephor of the 39th Ephoreia of Prehistoric and Classical Antiquities in Tripolis.

Susie Gillatt, scientific illustrator, was instrumental in transforming preliminary line drawings into the final illustrations, which appear here in this article.

Finally, I am touched by the hospitality and practical support provided by the residents and leadership of Ano Karyes. The accomplishments to date would have been much more difficult to achieve without such a base of operation with dedicated laboratory space close to the Sanctuary of Zeus.

References

Ambraseys, N. N., 1967, The earthquakes of 1965-66 in the Peloponnesus, Greece; a field report: Bulletin of the Seismological Society of America, v. 57, p. 1025-1046.

Ambraseys, N. N., and Jackson, J. A., 1990, Seismicity and associated strain of central Greece between 1890 and 1988: International Geophysical Journal, v. 101, p. 663-708.10.1111/j.1365-246X.1990.tb05577.x

Ambraseys, N., and Jackson, J., 1998, Faulting associated with historical and recent earthquakes in the Eastern Mediterranean region: International Geophysical Journal, v. 148, p. 390-406. 10.1046/j.1365-246X.1998.00508.x

Avramidis, P. and Zelilidis, A., 2001, The nature of deep-marine sedimentation and palaeocurrent trends as evidence of Pindos foreland basin fill conditions: Episodes, v. 24, no. 4, p. 252-256.

Baltuck, M., 1982, Provenance and distribution of Tethyan pelagic and hemipelagic siliceous sediments, Pindos Mountains, Greece: Sedimentary Geology, v. 31, no. 1, p. 63-88. 10.1016/0037-0738(82)90008-2

Briole, P., Rigo, A., Lyon-Caen, H., Ruegg, J. C., Papazissi, K., Mitsakaki, C., Balodimou, A., Veis, G., Hatzfeld, D., and Deschamps, A., 2000, Active deformation of the Corinth rift, Greece: Results from repeated Global Positioning System surveys between 1990 and 1995: Journal of Geophysical Research, v. 105, p. 25,605-25,625. 10.1029/2000JB900148

Bosellini, A., Winterer, E. L., 1975, Pelagic limestone and radiolarite of the Tethyan Mesozoic: a genetic model: Geology, v. 3, p. 279-28 10.1130/0091-7613(1975)3<279:PLAROT>2.0.CO;2

Clarke, P. J., Davies, R. R., England, P. C., Parsons, B., Billiris, H., Paradissis, D., Veis, G., Cross, P. A., Denys, P. H., Ashkenazi, V., Bingley, R., Kahle, H.-G., Muller, M.-V., and Briole, P., 1998, Crustal strain in central Greece from repeated GPS measurements in the interval 1989-1997: Geophysical Journal International, v. 135,p. 195-214. 10.1046/j.1365-246X.1998.00633.x

Cocard, M., Kahle, H.-G., Peter, Y., Geiger, A., Veis, G., Felekis, S., Paradissis, D., and Billiris, H., 1999, New constraints on the rapid crustal motion of the Aegean region: recent results inferred from GPS measurements (1993-1998) across the West Hellenic Arc, Greece: Earth and Planetary Science Letters, v. 172, p. 39-47. 10.1016/S0012-821X(99)00185-5

Degnan, P., and Robertson, A., 1994, Early Tertiary mélange in the Peloponnese (southern Greece) formed by subduction-accretion processes: Bulletin of the Geological Society of Greece, v. 30, p. 93-107.

Degnan, P. J., and Robertson, A. H. F., 1998, Mesozoic-early Tertiary passive margin evolution of the Pindos ocean (NW Peloponnese, Greece): Sedimentary Geology, v. 117, p. 33-70. 10.1016/S0037-0738(97)00113-9

Degnan, P. J., and Robertson, A. H. F., 2006, Synthesis of the tectonic-sedimentary evolution of the Mesozoic-early Cenozoic Pindos ocean; evidence from the NW Peloponnese, Greece: Geological Society Special Publications, v. 260, p. 467-491. 10.1144/GSL.SP.2006.260.01.19

Frazer, J.G. 1913, Pausanias's Description of Greece: MacMillan and Co., Ltd., London, 6 volumes.

Goldworthy, M., and Jackson, J. A., 2000, Active normal fault evolution in Greece revealed by geomorphology and drainage patterns: Journal of the Geological Society of London, v. 157, p. 967-981.

Goldworthy, M., and Jackson, J. A., 2001, Migration of activity within normal fault systems: examples from the Quaternary of mainland Greece: Journal of Structural Geology, v. 23, p. 489-506. 10.1016/S0191-8141(00)00121-8

Goldworthy, M., Jackson, J., and Haines, J., 2002, The continuity of active fault systems in Greece: International Geophysical Journal, v. 148, p. 596-618. 10.1046/j.1365-246X.2002.01609.x

Golonka, J., 2004, Plate tectonic evolution of the southern margin of Eurasia in the Mesozoic and Cenozoic: Tectonophysics, v. 381, p. 235-273. 10.1016/j.tecto.2002.06.004

Jackson, J., 1994, Active tectonics of Aegean region: Annual Review of Earth and Planetary Science, v. 22, p. 239-271. 10.1146/annurev.ea.22.050194.001323

Jackson, J., and McKenzie, D., 1999, A hectare of fresh striations on the Arkitsa fault, central Greece: Journal of Structural Geology, v. 21, p. 1-6. 10.1016/S0191-8141(98)00091-1

Jackson, J. A., Gagnepain, J., Houseman, G., King, G. C. P., Papadimitrious, P., Soufleris, C., and Virieux, J., 1982, Seismicity, normal faulting, and the geomorphological development of the Gulf of Corinth (Greece): the Corinth earthquakes of February and March 1981: Earth and Planetary Science Letters, v. 57, p. 377-397. 10.1016/0012-821X(82)90158-3

Jolivet, L., and Patriat, M., 1999, Ductile extension and the formation of the Aegean Sea, in Durand, B., Jolivet, L., Horvath, F., and Seranne, M., eds., The Mediterranean basins: Tertiary extension within the Alpine orogen: Geological Society of London Special Publication 156, p. 427-456.

Jolivet, L., Famin, V., Mehl, C., Parra, T., Aubourg, C., Hebert, R., and Philippot, P., 2004, Strain localization during crustal-scale boudinage to form extensional metamorphic domes in the Aegean Sea, in Whitney, D. L, Teyssier, C., and Siddoway, C. S., Gneiss domes in orogeny: Geological Society of America Special Paper 380, p. 185-210.

Kissel and others, 1984

Kourouniotis, K., 1903, Ανασκαφή Λυκαίου: Praktika, p. 50-52.

Kourouniotis, K., 1904, Ανασκαφή Λυκαίου: Praktika, p. 32-34.

Kourouniotis, K., 1905, Ανασκαφή Λυκαίου: ArchEph, p. 161-78.

Kourouniotis, K., 1909, Ανασκαφή Λυκαίου: Praktika, p. 185-200.

Lalechos, N., 1973, Geological map of the Greece Kato Fighalia Sheet (1:50,000): National Institute of Geological and Mining Research.

Le Pichon, X., Chamot-Rooke, N., and Lallemant, S., 1995, Geodetic determination of the kinematics of central Greece with respect to Europe: implications for eastern Mediterranean tectonics: Journal of Geophysical Research, v. 100, p. 12,675-12,690.

Lister, G. S., Banga, G., and Feenstra, A., 1984, Metamorphic core complexes of Cordilleran type in the Cyclades, Aegean Sea, Greece: Geology, v. 12, p. 221-225. 10.1130/0091-7613(1984)12<221:MCCOCT>2.0.CO;2

McClusky, S., Balassanian, S., Barka, A., Demir, C., Ergintav, S., Georgiev, I., Gurkan, O., Hamburger, M., Hurst, K., Kahle, H.-G., Kastens, K., Kekelidze, G., King, R., Kotzev, V., Lenk, O., Mahmoud, S., Mishin, A., Nadariya, M., Ouzounis, A., Paradissis, D., Peter, Y., Prlepin, M., Reilinger, R., Sanli, I, Seeger, H., Tealeb, A., Toksoz, M., and Veis, G., 2000, Global Positioning System constraints on plate kinematics and dynamics in the eastern Mediterranean and Caucasus: Journal of Geophysical Research, v. 105, p. 5695-5719.

McKensie, D., 1970, Active tectonics of the Mediterranean region: Nature, v. 226, p. 239-243. 10.1038/226239a0

PMid:16057188

McKenzie, D., 1978, Active tectonics of the Alpine-Himalayan belt: the Aegean Sear and surrounding regions: Geophysical Journal of the Royal Astronomical Society, v. 55, p. 217-254.

Morewood, N. C., and Roberts, G. P., 2001, Comparison of surface slip and focal mechanism slip data along normal faults: an example from the eastern Gulf of Corinth, Greece: Journal of Structural Geology, v. 23, p. 473-487. 10.1016/S0191-8141(00)00126-7

Oral, M B., Relinger, R. E., Toksoz, M. N., King, R. W., Barka, A. A., Kinik, I., and Lenk, O., 1995, Global Positioning System offers evidence of plate motions in eastern Mediterranean: EOS, Transactions, American Geophysical Union, v. 76.

Papadopoulos, P., 1997, Geological Map of the Megalopolis Sheet (1:50,000; 40 m contour interval): Institute of Geology and Mineral Exploration.

Pe-Piper, G., and Piper, D. J. W., 1984, Tectonic setting of the Mesozoic Pindos Basin of the Peloponnese, Greece: Geological Society Special Publications, v. 17, p. 563-567. 10.1144/GSL.SP.1984.017.01.43

Piper, D. J. W., 2006, Sedimentology and tectonic setting of the Pindos Flysch of the Peloponnese, Greece: Geological Society Special Publications, v. 260, p. 493-505. 10.1144/GSL.SP.2006.260.01.20

Ramsay, J. G., 1974, Development of chevron folds: Geological Society of America Bulletin, v. 85, p. 1741-1753. 10.1130/0016-7606(1974)85<1741:DOCF>2.0.CO;2

Reilinger, R. E., McClusky, S. C., Oral, M. B., King, R. W., Toksoz, M. N., Barka, A. A., Kinik, I., Lenk, O., and Sanli, I., 1997, Global Positioning System measurements of present-day crustal movements in the Arabia-Africa-Eurasia plate collision zone: Journal of Geophysical Research, v. 102, no. 9983, p. 9983-9999. 10.1029/96JB03736

Richter, D., and Mueller, C., 1993, Der “Erste Flysch” in der Pindos-Zone (Griechenland): Neues Jahrbuch fuer Geologie und Palaeontologie, v. 1993, no. 4, p. 209-226.

Roberts, G. P., 1996, Noncharacteristic normal faulting surface ruptures from the Gulf of Corinth, Greece: Journal of Geophysical Research, v. 101, p. 25,255-25,267. 10.1029/96JB02119

Roberts, G., and Stewart, I., 1994, Uplift, deformation and fluid involvement within an active normal fault zone in the Gulf of Corinth, Greece: Journal of the Geological Society of London, v. 151,p. 531-541. 10.1144/gsjgs.151.3.0531

Roberts, G. P., and Ganas, A., 2000, Fault-slip directions in central and southern Greece measured from striated and corrugated fault planes: Comparison with focal mechanism and geodetic data: Journal of Geophysical Research, v. 105, p. 23,445-23,462. 10.1029/1999JB900440

Roberts, S. and Jackson, J., 1991, Active normal faulting in central Greece: an overview: Geological Society of London Special Publication 148, p. 125-142.

Robertson, A. H. F., and Dixon, J. E., 1984, Introduction: aspects of the geological evolution of the Eastern Mediterranean: Geological Society, London, Special Publications, v. 17, p. 1-74.

Romano, D.G. 1981. The stadia of the Peloponnesos. [Ph.D. dissertation]: University of Pennsylvania (Philadelphia), Ann Arbor, pp. 172-177.

Romano, D. G., 1997. Topographical and architectural survey of the sanctuary of Zeus on Mt. Lykaion, Arcadia: American Journal of Archaeology, v. 101, p. 374.

Skourlis, K., and Doutsos, T., 2003, The Pindos fold-and-thrust belt (Greece); inversion kinematics of a passive continental margin: International Journal of Earth Sciences, v. 92, no. 6, p. 891-903. 10.1007/s00531-003-0365-4

Sorel, D., 2000, A Pleistocene and still-active detachment fault and the origin of the Corinth-Patras rift, Greece: Geology, v. 28, p. 83-86. 10.1130/0091-7613(2000)28<83:APASDF>2.0.CO;2

Stewart, I. S., and Hancock, P. L., 1988, Normal fault zone evolution and fault scarp degradation in the Aegean region: Basin Research, v. 1, p. 139-154.

Stewart, I. S., and Hancock, P. L., 1991, Scales of structural heterogeneity within neotectonic normal fault zones in the Aegean region: Journal of Structural Geology, v. 13, p. 191-204. 10.1016/0191-8141(91)90066-R

van Hinsbergen, D. J. J., 2005, Nappe stacking resulting from subduction of oceanic and continental lithosphere below Greece: Geology, v. 33, p. 325-328. 10.1130/G20878.1

van Hinsbergen, D. J. J., 2006, Deformation of western Greece during Neogene clockwise rotation and collision with Apulia: International Journal of Earth Sciences (Geologische Rundshau), v. 95, p. 463-490. 10.1007/s00531-005-0047-5

Walgreich, M., Pavlopoulos, A., Faupl, P., and Migiras, G., 1996, Age and significance of upper Cretaceous siliclastic turbidites in the central Pindos Mountains, Greece: Geological Magazine, v. 133, p. 325-331. 10.1017/S0016756800009055

Wilford, J. N., February 5, 2008, An altar beyond Olympus for a deity predating Zeus: New York Times, Science.

A. Field Guide to the Geology of the Sanctuary of Zeus, Mt. Lykaion, The Peloponessos

Introduction

This field trip guide presupposes that the reader has become reasonably familiar with the descriptions and interpretations of rocks, structures, and geoarchaeology that are provided in the preceding text, and/or has grasped the framework of the text and can "dig" efficiently for details. As an aid to "mining" the text for details while in the field, this guide is sprinkled liberally with cross-references to pertinent sections of the text.

Figure FT-1 is a map showing all of the stops in this field guide. Figure FT-2 is the geologic map, and it also shows the locations of stops. [Section VII of companion paper covers "Geologic Mapping Of The Sanctuary"].

Stop A, the first stop of the trip, is a vista from the village of Kastanochori. Figure FT-3 and Table 1 describe how to reach Stop A, starting from the platea in the center of Megalopolis. Kastanochori is a small mountain village located on a winding narrow road. Midway through the village you will approach a sharp left-hand turn. The paved road at this point is simply one lane. You will spot the turn from a distance, because there is a conspicuous circular mirror angled to allow you to see if any cars are about to come around the blind turn. Once you have safely made the left-hand turn you will be on a straight stretch of narrow road for ~50 m, and then the road suddenly widens in ways that provide for plenty of room to park safely on the left. This is Stop A.

Figure FT01. Google image, showing location of field trip stops.

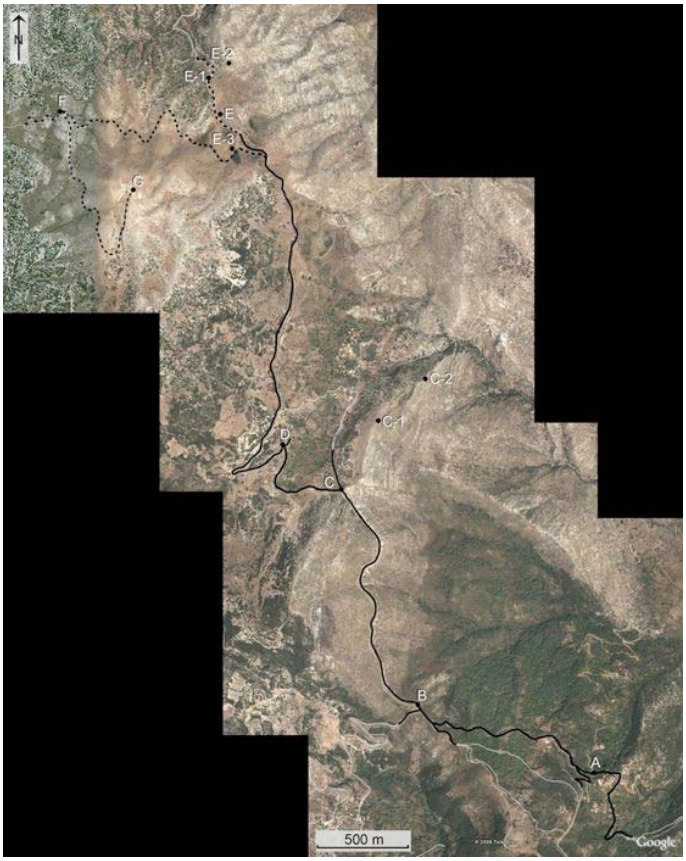

Map of the locations of the field-trip Stops.

Figure FT02. Geologic map, showing location of field trip stops.

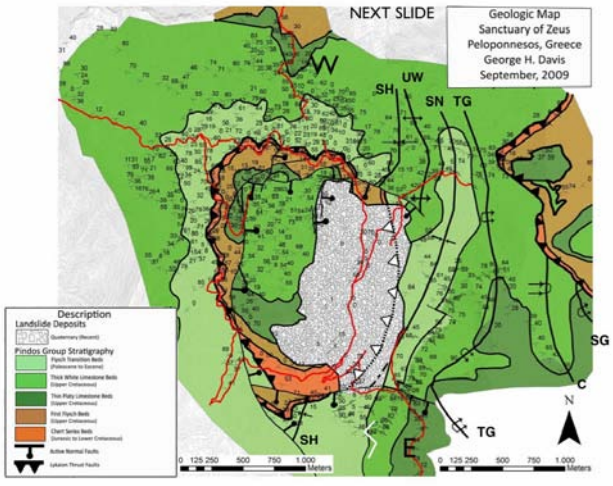

Geologic map of the study area, showing locations of Stops.

Figure FT03. Google map, showing directions to Stop A from Megalopolis.

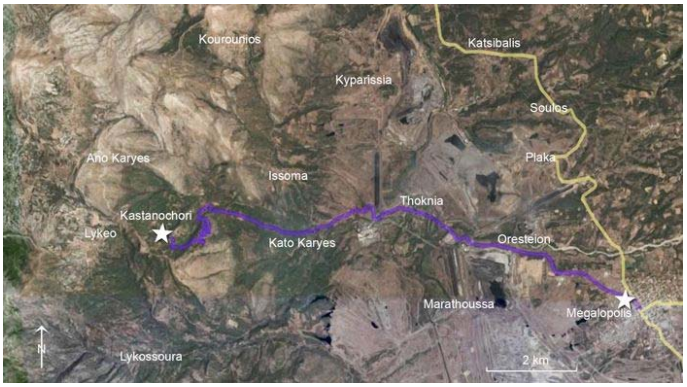

Map showing route from the platea, in the center of Megalopolis, to Stop A, on the western edge of the village of Kastanochori.

Stop A.

Cross over to the north side of the road, looking carefully for cars that might be moving swiftly on this mountain road. The view to the north is parallel to the structural grain of the Pindos fold and thrust belt (Figure FT-4). This is a good vantage to gain a sense for the size and style of folding that dominates the structural geology of the eastern third of the map area, and to spot a trace of the Lykaion thrust in the far distance. Furthermore, from here we can begin to appreciate the landscape expressions of First Flysch Beds, Thin Platy Limestone Beds, and Thick White Limestone Beds. [Section VI of the companion paper describes “Stratigraphy Within The Sanctuary of Mt. Lykaion"].

Figure FT04. View from Stop A of major folding.

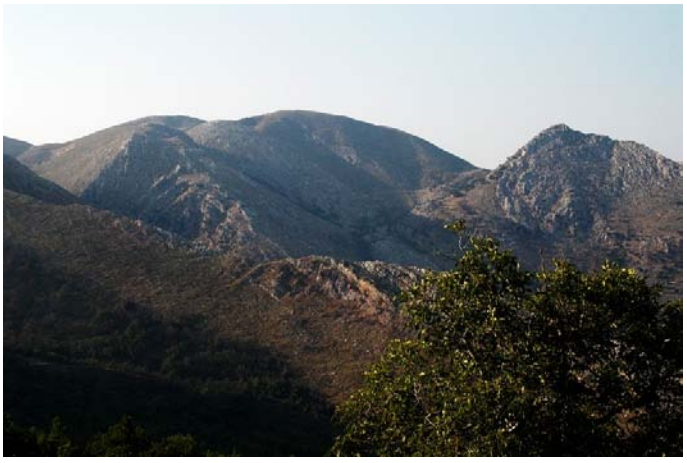

Photograph directed northward from Kastanochori. Limestone capping ridge in foreground is part of the Thick White Limestone Beds. The grass and brush-covered slope below and to the left is underlain by Thin Platy Limestone Beds. Further downslope is a burnt woods underlain by First Flysch Beds. In left background the Three Gorges anticline is clearly evident. On far right in background is the westward-overturned St. George anticline. In far center background is the hill in which the Lykaion thrust fault is exposed.

Spotting the trace of the Lykaion thrust from here will be important. It dips very gently eastward and is marked by stark contrast between dark rocks above and white rocks below (see Figure 26). Above this thrust is the Zeus thrust sheet. Below this thrust is the Pan thrust sheet. Almost all of the rocks that comprise this view from Stop A belong to the Pan thrust sheet. The Sanctuary of Zeus is not visible from here, nor is the St. Elijah klippe. [Section VII-B1 in companion paper covers “Overall Structural Relationships].

Consult the geologic map (see Figure FT-2) to note the locations and orientations of the five major fold structures in the eastern third of the study area, and the location of the Lykaion thrust fault. [Section VII-C1 in the companion papers covers “Overall Structural Relaions” in this eastern domain].

Looking north from Stop A, you will see a profile view of the Three Gorges anticline (see Figure FT-4). Furthermore, you will see the overturned western limb of the St. George anticline (see Figure FT-4). On its pointed summit is the tiny chapel to St. George (Figure FT-5). On the highest ridge in the distance is the trace of the Lykaion thrust fault, which here dips gently eastward (see Figure FT-4). The dark-colored hanging-wall rocks that you see there are primarily First Flysch Beds (i.e., brown sandstones). The white footwall rocks are Thick White Limestone Beds.

Figure FT05. View of peak on which St. George Chapel is located.

A. East-directed view of hill spire on top of which is located the Chapel of St. George.

B. Close-up view of the St. George Chapel.

This is a good place to begin to gain a sense for the landscape expression of some of the rock formations (see Figure FT-4). In the foreground, i.e., from the road down across the tree-covered slopes to the first major canyon, the landscape expression of First Flysch Beds is well displayed. In contrast, the stark bedrock landscapes in the middle and far distance are underlain by Thin Platy Limestone Beds and overlying Thick White Limestone Beds (see Figure FT-4). Thick White Limestone Beds is bright white and very resistant to erosion. Its expression is particularly pronounced on the highest ridges, cropping out in massive craggy layers. The bedrock on Agios Georgios is Thick White Limestone Beds. The large folds that are evident from this vista occupy the Hippodrome thrust sheet, which lies below the Lykaion thrust and the Lykaion klippe (see Figure FT-2).

Now head 1.2 km up the road to Stop B.

Stop B.

Stop B is located at a fork in the road (see Figures FT-1, 2). Park in a way that it will be easy, following this stop, to take the right fork and continue up the mountain.

Though you will see outcrops of brown sandstone belonging to First Flysch Beds right at the fork, the purpose of this stop is to examine the character of Thin Platy Limestone Beds. This formation is very well exposed in the roadcuts as you walk up the road, in an easterly direction. If you walk up the road and examine these roadcut outcrops for a distance of ~100 m, you will develop a clear picture of the properties of Thin Platy Limestone Beds.

There are a number of interesting characteristics of the Thin Platy Limestone Beds that can be seen at Stop B (Figure FT-6): 1/ the thin, platy bedded character of this formation; 2/ concordant bedding-parallel lenses and layers of white and black chert; 3/ closely spaced jointing; and 4/ tight, strongly overturned chevron folds. Folding appears to have been produced by flexural slip mechanisms. [Section VI-D of companion paper describes Thin Platy Limestone Beds].

Figure FT06. Outcrop expression of Thin Platy Limestone Beds near Stop B.

Thin Platy Limestone Beds exposed in the vicinity of Stop B. Phil Nickerson is the geologist. Note the tight chevron folding of bedding and the intensely fractured nature of the limestone beds.

Now head 1.49 km up the road to Stop C.

Stop C.

Stop C is at a fork in the road, and it is easy to spot because of the tiny chapel, called Agios Nikolaos, the Chapel of St. Nicholas (Figure FT-7), which is located at Stop C (see Figures FT-1, 2).

Figure FT07. View of St. Nicholas Chapel, and Stop C, from above.

A. Northeast-directed view of Stop C. Although this image resembles an aerial photograph, the location from where I took this photo is the top of a tall, steep-sided ridge. My companions during this shooting are in Figure FT-7B. Note the red-tiled roof of the Chapel of St. Nicholas. All of the bold limestone bedrock belongs to Thick White Limestone Beds. The grassy areas are underlain by Flysch Transition Beds. Note the traces of compartmental faulting that shifts the contact between the two Pindos Group formations exposed near Stop C.

B. Goats high above Stop C.

The bedrock at this location is Thick White Limestone Beds. The properties of this formation are exquisitely displayed in outcrops behind (i.e., north of) the chapel (Figure FT-8). In particularly you will see that bedding is steeply inclined and marked by pervasive stylolite dissolution, producing stylobedding. The bedding is strongly folded, and the folds tend to be overturned to recumbent (see Figure FT-8). All of these strata occupy the Pan thrust sheet.

Figure FT08. Folded Thick White Limestone Beds behind St. Nicholas Chapel.

Folded limestone beds on north side of the Chapel of St. Nicholas. This is the western overturned limb of the St. Nickolas syncline. The formation is Thick White Limestone Beds.

If you 'backtrack' down the hill for ~100 m or so, you will be able to see the zone of contact between Thin Platy Limestone Beds and the Thick White Limestone Beds. (The pink/purple beds belong to Thick White Limestone Beds formation). If you stand in the small parking area south of the chapel and look southwest toward and up the ridge which is south of the road, you will see a good example of the landscape expressions of both of the limestone formations. What is striking is that Thin Platy Limestone Beds, so apparently resistant in roadcuts, has very poor outcrop expression on the steep hillslopes. It weathers into a blocky, rubbly, grass-covered slope. In contrast, the beds within Thick White Limestone Beds crop out like resistant struts with significant continuity, and they stand out in sharp contrast with "furrows" along the traces of weaker lithologies within this formation (Figure FT-9). [Section VI-E of the companion paper describes "Thick White Limestone Beds].

Figure FT09. Landscape expression of Thick White Limestone Beds.

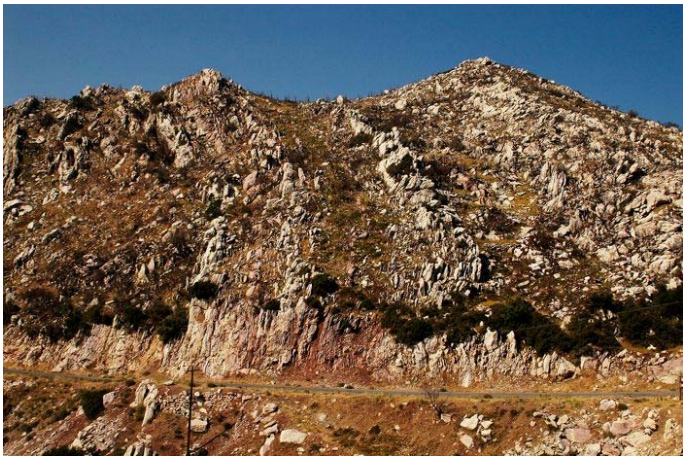

Southwest-directed views of landscape expression of Thick White Limestone Beds. Note "furrows" that are underlain by weak mudstone interbeds.

For those who have the time and interest, head northward from Stop C to Stops C1 and C2. Start off on the path that comes out of the brush on the north side of the chapel near the road. Once beyond the thick brush you will see that the landscape opens up, and in fact you will find yourself going along the edge of a shallow grassy sinkhole depression. From Stop C, you will be walk northward along the ridge crest for ~0.5 km; your 'target' (Stop C1) is a 2m-high geodetic monument that can be spotted from some distance away. The monument is called Pseiliko, and registers an elevation of 1039.82 m.

Stop C1.

From the location of the monument look generally westward (Figure FT-10) where you will see the village of Ano Karyes (see Figures FT-1, 2). Ano Karyes has been the base of field operations for the Mt. Lykaion Excavation and Survey Project. On the skyline to the west you will see a white cliff face, beneath which are large scree slopes (see Figure FT-10). The cliff and scree slopes are expressions of the active fault system bordering the eastern edge of the St. Elijah klippe, which strikes NNE, dips ESE. The normal faulting accommodated by this fault system has incrementally dropped the high-plateau upland of Mt. Lykaion to lower and lower elevations, in part through a series of fault-bounded steps. The rocks of this high-plateau upland are part of the Zeus thrust sheet, though this is not obvious from here, for the trace of the Lykaion thrust fault is covered by landslide deposits. [Section VII-D3 of the companion paper describes "Active Faulting Bordering St. Elijah Klippe on East"].

Figure FT10. View from C-1 toward Ano Karyes and landslides above.

Photograph showing view to the west from Pseiliko. In the foreground is a part of the village of Ano Karyes. In the distant background is the eastern precipitous margin of Agios Elias. This boundary is demarcated by active normal faulting. Oversteepening by faulting is creating landslides and rock falls, as can be seen from great distances away.

The white cliff face is composed both of Thick White Limestone Beds and landslide colluvium. The northernmost and westernmost parts of the village of Ano Karyes appear to be built on top of a mantle of coalescing landslides. As is the case throughout Arcadia, earthquakes impose greatest damage on houses and villages built on landslides. This certainly was true of the Megalopolis earthquake in 1965.

Stop C2.

For those who have the time and stamina, proceed now to Stop C2 by walking north-northeast for ~0.4 km (see Figures 1, 2). Though Stop C2 is plotted as a discrete point on the map (see Figure FT-1), the objective is to walk around to places where there are good views of folding. The Three Gorges anticline (Figure FT-11) can be seen to the north, as expressed in Thick White Limestone Beds on the south-facing wall of a deep canyon (Figure FT-11. Steeply dipping overturned strata of the St. George anticline can be seen to the northeast (see Figures FT-4 and FT-5). Now, turning southward, the near-isoclinal Cretea syncline may be evident (Figure FT-12). (Gaining a clear view of the Cretea syncline may require contouring southeastward to the top of the next ridge). The bedrock within this syncline consists of Thick White Limestone Beds and Thin Platy Limestone Beds (Figure FT-12). This combination of views, in concert with examination of the geologic map (see Figure FT-2), offers an excellent picture of the macroscopic folding within the Pan thrust sheet. This folding is intimately related to thrust faulting and crustal shortening of Pindos group sediments that took place from late Cretaceous through Oligocene.

Figure FT11. View of Three Gorges anticline and St. George's spire

In the foreground is the expression of the Three Gorges anticline. In the background is the hilltop spire on top of which is built the St. George Chapel. The chapel lies close to the trace of the St. George (overturned) anticline.

Figure FT12. View of Cretea syncline.

South-directed view of the Cretea syncline. The eastern limb is overturned. Strata in right foreground are Thick White Limestone Beds.

Now return to the vehicles and drive westward from the Chapel of St. Nicholas to Stop D, a distance of 0.8 km.

Stop D.

This is Krabova spring (Figure FT-13). Stopping here has become a daily routine for those of us engaged in the Mt. Lykaion Excavation and Survey Project (see Figures FT-1, 2). The water is delicious. It is a good place to fill up water bottles. There are numerous springs on the east flank of Mt. Lykaion. Many of them issue from the landslide colluvium, which seems to be able to retain a lot of water. The spring system on this part of the mountain is, of course, responsible for the place of settlement of Ano Karyes and the positioning of its orchards and fields.

Figure FT13. Krabova spring in background. [this is a place-holder].

South-southeast-directed view of Krabova spring, which is in the foreground (immediately south of built structure with red tile roof). Landslide complex in background is primarily composed of mass-wasted Thin Platy Limestone Beds.

Proceed up the mountain for ~2.7 km, where you will enter the lower sanctuary area. Ignore for now the sharp left turn, which (later) will take you up to Agios Elias, the second highest summit of Mt. Lykaion. Instead, continue straight ahead at the fork, drive down and onto the gray cinder track, which is the site where the modern Lykaion games are held. Park near the end of the track, at Stop E. The structural position you now occupy is one immediately below the Lykaion thrust fault in the uppermost part of the Pan thrust sheet. [Section I of companion paper is the "Introduction," which conveys Pausanias' early descriptions of the sanctuary; section II, "Purpose of the Paper," gives information regarding the arrangement of the archaeological elements].

Stop E.

Stop E is located near the base of the processional way near the southern end of the hippodrome (see Figures FT-1, 2). The cinder track represents only ~15% of the total area of the hippodrome; most of the hippodrome extends north of the cinder track. A thin layer of silt and clay covers the actual surface of the hippodrome; the silt and clay represent an influx since the time of last use of the hippodrome.

To gain perspective on the nature of the lower sanctuary it is useful to walk north along the dirt road and the hippodrome proper for 025 km to

(Figure FT-14; see also Figures FT-1, 2). In doing so you will begin to appreciate the flat nature of the hippodrome space, especially in contrast to the general topography of the mountain. You will also be able to see the location of the ancient retaining wall built along the eastern margin of the hippodrome. The bath is located just beyond the north end of the hippodrome (see Figure FT-2), and the blocks used in construction of it are derived from Thick White Limestone Beds (Figure FT-15).

Figure FT14. North view from Agios Elias to lower sanctuary area.

North-directed view from the flank of Agios Elios across the hippodrome to the area of the bath. In the foreground, the grass-covered hills are mainly underlain by First Flysch Beds. These occupy the Zeus thrust sheet. The segment of road in the near middle ground crosses the upper part of the Pan thrust sheet just below the Lykaion thrust fault. Bedrock exposed next to the road is Flysch Transition Beds. The ridge descending from the road to the flat expanse is the processional ridge. The middle ground and distant ground on the extreme left exposes Thick White Limestone Beds. The cinder track (dark gray) in right middle ground is the site of athletic competitions associated with the modern Lykaion games. It covers the southernmost part of the hippodrome. Most of the hippodrome lies north-northwest of the cinder track; it is a grass-covered expanse, but also contains on the order of twenty trees. Note a straight line separating dark green grass (on to the west) from lighter grass (on the east). This is the location of the retaining wall for the hippodrome. The bath is located just off the northeastern corner of the hippodrome. North of the baths is sink-hole hill.

Figure FT15. Bath near hippodrome.

Close-up view of baths, with walls composed of blocks of Thick White Limestone Beds. Geologist is Karl Yares.

Hike northward ~0.2 km the hill to the location of Stop E2. The bedrock is Thick White Limestone Beds. If you choose to hike all the way to the top of this hill you will see that there is a find a sink hole at the crest (see Figure FT14). From anywhere on the slope where Stop E1 is designated, there are perfect south-directed views of the layout of the Sanctuary of Zeus, Mt. Lykaion, and its underlying geology (Figure FT-16). The highest point on the south horizon is the ash altar, at the very top of Agios Elias. The hippodrome and bath are in the immediate foreground. Above the level of the hippodrome near the base of Agios Elias is the trace of the Lykaion thrust fault (see Figure FT-16). This fault stands out sharply, in part because the modern road near the base of the northern slope of Agios Elias follows closely the trace of the Lykaion thrust fault. The landscape above the trace of the thrust is occupied by the Zeus thrust sheet in general, and the St. Elijah klippe in particular. Agios Elisas is smooth and rounded, locally rilled, and underlain dominantly by First Flysch Beds. Bedrock exposures are meager. In contrast, directly below the Lykaion thrust is a landscape dominated by limestone outcrops within the Pan thrust sheet (see Figure FT-16). The limestone just below the thrust belongs to the Flysch Transition Beds. Beneath the Flysch Transition Beds are Thick White Stylolite Beds. Not particularly visible from this vantage is the presence of Chert Series Beds in the immediate hanging wall of the Lykaion thrust fault.

Figure FT16. South view from Stop E2 toward lower sanctuary area.

South directed view of lower sanctuary from sink-hole hill. The baths are in the immediate middle foreground. The trace of the Lykaion thrust fault essentially runs along brown-purple road in background and separates the Zeus thrust sheet (above) from the Pan thrust sheet (below). The hippodrome is in the right middle-ground. The gray, cinder part of the hippodrome is the track used for the Modern Lykaion Games. Just beyond the cinder track are the excavations of the lower sanctuary (the stoa location, marked by abundant white limestone blocks, lies just beneath the brown-purple road). Limestone outcrops on the far horizon are mainly Thick White Limestone Beds. Much of the St. Elijah klippe in this particular view is underlain by First Flysch Beds. The reddish soil/rock immediately above the road is the expression of Chert Series Beds.

From the vantage of Stop E2 it is possible to appreciate the structural geological location of the area containing the stoa, xenon, seating area, and stoa spring (Stop E3; see Figures FT-2). These built structures occupy the uppermost part of the Pan thrust sheet and are located just beneath the Lykaion thrust fault (see Figure FT-15). Furthermore, the geomorphic character of the processional way can be appreciated from Stop E2 (see Frontispiece).

Depending on time and interest, there are two routes to Stop E3. The easiest and shortest way is to head southwest to the dirt road that runs along the west side of the hippodrome. There are good bedrock exposures in the roadcuts. In walking south along this road, you will go from Thick White Limestone Beds to Flysch Transition Beds (see Figure FT-2). The longer route is to head southeast from Stop E2 and eventually climb up onto the ridge of limestone east of the hippodrome (see Figure

FT-14). In so doing you will have a chance to see typical outcrop expressions of Thick White Limestone Beds, and to cross into and see the properties of Flysch Transition Beds (see also Figure FT-2). The Flysch Transition Beds formation has thinner and smoother bedding than the Thick White Limestone Beds. Furthermore, there are distinctive layers of bedded black chert in the Flysch Transition Beds (Figure FT-17). The total distance of this leg of the walk is ~0.6 km.

Figure FT17. Black chert layer within Flysch Transition Beds.

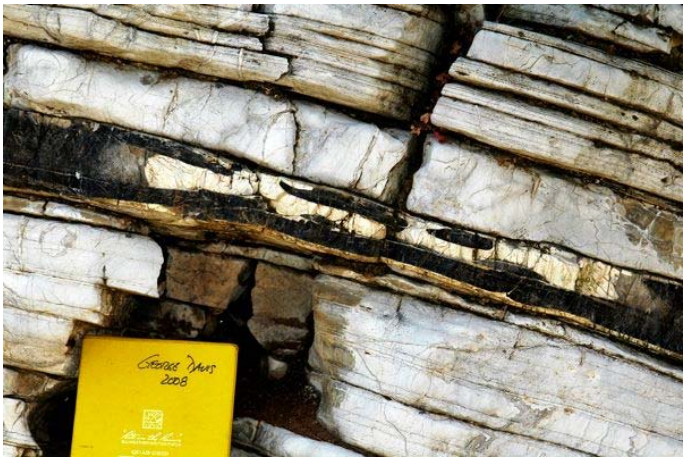

Photography of outcrop of limestone beds and black chert layers within the Flysch Transition Beds.

Stop E3.

At Stop E3 you will be able to see the stoa, seating, xenon, and a fountain house for a spring (Figure FT-18A; see also Figures FT-1, 2). Nearly all of the blocks that were worked and placed to form these built structures are derived from Thick White Limestone Beds (Figure FT-18B). It is interesting to examine the fabrics and structures that are evident in the blocks, especially the abundant stylolites, en echelon gash veins, and crystal-fiber veins.

Figure FT18. View of seatwall and stoa.

A. East-directed photograph of built structures within the lower sanctuary. The red road cut in background is a useful reference, for it is composed of sheared, weathered Chert Series Beds, which comprise the immediate hanging wall of the Lykaion thrust. The trace of the thrust itself runs along the uppermost part of the near bank of the road, just above the backwall of the stoa, whose large rectangular footprint is strewn with worked blocks of Thick White Limestone Beds. On the next terrace down is a long narrow rectangular seating area (or steps) also comprised of worked blocks of Thick White Limestone Beds. Of the two spire-like hills in the background, the one on the left is the hill on which the tiny chapel to St. George was built.

B. Photograph of a part of the backwall of the stoa. The worked limestone blocks are from Thick White Limestone Beds.

Geologically the most important part of Stop E3 is to gain a sense of the location and character of the Lykaion thrust fault. To do so, proceed east to the fork in the road, and then begin to walk up the road. As you do so you will walk along the eastern back wall of the stoa. The

outcrops you see in the roadcuts display the characteristic red-purple hue of Chert Series Beds, which occupy the Zeus thrust sheet directly about the fault. In places you will see some displays of radiolarian (ribbon) cherts within the Chert Series Beds, but the outcrop quality is not nearly as good as what we will see later. Above the road, on the hill slopes, are abundant resistant outcrops and benches of brown sandstones of the First Flysch Beds (Figure FT-19). Below the road are spotty but distinctive outcrops of rocks of the lower thrust sheet, namely limestones of the Flysch Transition Beds. [Section VI-B of the companion paper gives descriptions of the "Chert Series Beds;" section VI-C gives descriptions of the "First Flysch Beds"].

Figure FT19. Seatwall in foreground, St. Elijah klippe in background.

South-directed photograph toward Agios Elios, and the St. Elijah klippe. In foreground Pam Jordan draws limestone blocks comprising the seat wall in the lower part of the sanctuary. Beyond her in the middle ground are foundation walls of the xenon. The road in the background 'travels' right along the Lykaion thrust fault. Note reddish material on right in the roadcut. This rock belongs to the Chert Series Beds. Above the Chert Series Beds and making up much of the lower reaches of the klippe is First Flysch Beds. The brown sandstone layers within the First Flysch Beds crop out as bedrock hummocks of resistant though jointed rock.

Now return to the vehicles and begin driving to Stop F (see Figure FT-1). It is an ~1.5 km drive.

Proceeding from Stop E to Stop F.

Throughout much of this stretch of dirt road you are driving essentially along the trace of the Lykaion thrust fault (see Figures FT-2 and FT-14). This will be evident because of the striking contrast between the limestone-rich bedrock of the Flysch Transition Beds that occupies the top of the Pan thrust sheet, and the distinctive lithologies of the Chert Series Beds and First Flysch Beds that occupy the lower part of the Zeus thrust sheet. Within the Chert Series Beds the dominant lithologies are ribbon cherts and red mudstones. Within the Flysch Transition Beds the dominant lithology by far is gray limestone.

The geological properties of some of the outcrops in the roadcuts will attract your attention, especially, for example, where the Chert Series Beds are profoundly sheared and folded, and where the Flysch Transition Beds display a 'tombstone topography' marked by clear outcrop expression of thin beds of dipping limestone.

Stop F.

Stop F is located at yet another fork in the road (see Figure FT-1). Find a place to stop near the fork, and then walk around and look around to gain a sense for the geology in the northwestern part of the map area (see Figure FT-2). For example, to the north and northwest are tree- and brush-covered ridges with bold expressions of Thick White Limestone Beds (Figure FT-20). Yet in the vicinity of Stop F the bedrock is Flysch Transition Beds, consisting of interbedded limestone, sandstone, siltstone, and mudstone. Folding is particularly evident in the Flysch Transition Beds. Locally there is a one-to-one relationship between N-S-trending (narrow) ridges and N-S-trending (tight) anticlines (FT-21). In between are low areas (synclines) marked by terraced agricultural fields. These are unusual examples of structural control of farm fields. [Section VI-F of the companion paper provides descriptions of the "Flysch Transition Beds"].

Figure FT20. Characteristic landscape of Thick White Limestone Beds.

Northwest-directed photographs of broad expanses of Thick White Limestone Beds. The bedrock is ragged and difficult to negotiate in places, especially where vegetation is thick. By comparison, the landscape underlain by Flysch Transition Beds (in foreground) is smooth and broadly rolling.

Figure FT21. View of coordinated array of folds and fields.

South-directed photographs of folded Flysch Transition Beds. Note that the prominent limestone ridge is an upright anticline defined by resistant limestone. The terraced areas on either side of the anticlinal ridge are traces of synclines.

Now return to your vehicle(s).

Proceeding from Stop E to Stop F.

Along this stretch of road you will pass upward through the uppermost part of the Pan thrust sheet and cross the Lykaion thrust fault, thus entering the overlying Zeus thrust sheet. You start out in Flysch Transition Beds located in the upper part of the Pan thrust sheet (see Figures FT-1, 2). The Flysch Transition Beds are easy to recognize, marked by abundant limestone bedrock in roadcuts (Figure FT-22). You will see these outcrops for the first ~0.4 km of the drive toward Stop F. You might pause at the 0.4 km mark and get out to look at the horse pasturing area, the broad field off to the south-southwest. If you have time, it is a pleasant experience to walk this pasture field, and check out the beautiful fold structures in Thick White Limestone Beds at the far southerly end of the filed (Figure FT-23).

Figure FT22. Exposures of Flysch Transition Beds.

Outcrop expression of Flysch Transition Beds along road. The limestone beds bear a similarity to those of the Thin Platy Limestone Beds, but there are significant differences, including the abundance of interbedded mudstones and siltstones.

Figure FT23. Folds in Thick White Limestone Beds south of horse pasture.

South-directed photo of southernmost part of the horse pasture field. Note folds in limestone beds, which belong to Thick White Limestone Beds.

The part of the road you are ascending is pictured in Figure FT-23. Limestone outcrops of the Flysch Transition Beds are in the foreground and in the left middle ground. Upward and southward along the road, the Flysch Transition Beds formation gives way to the Chert Series Beds (see Figure FT-24). Specifically, at the ~0.7 km mark on the drive from Stop E to Stop F, the character of bedrock abruptly changes, where the road crosses the Lykaion thrust fault. The bedrock shifts from limestone to highly sheared and folded Chert Series Beds, which occupy the lowermost part of the Zeus thrust sheet (Figure FT-25). In particular there are excellent displays of ribbon cherts (replete with penetrative jointing) that locally are intensely folded. Between ribbons is sheared red mudstone, which locally contains rootless isoclinal folds, revealing that the Chert Series Beds is partly transposed.

Figure FT24. View of Agios Elias and trace of Lykaion thrust fault.

A. East-directed view of road ascending Agios Elios. In the foreground and left middle ground are limestone outcrops representing the Flysch Transition Beds. Along the road, the change from limestone to red mudstones and chert layers signals crossing the Lykaion thrust fault. Above the thrust is the St. Elijah klippe.

B. Closer east-directed view of road ascending Agios Elios. In the right foreground and middle ground are limestone outcrops representing the Flysch Transition Beds. These are part of the Pan thrust sheet. The red-purple beds in the left middle ground are Chert Series Beds within the Zeus thrust sheet. The brown-weathering rock further up the road (right middle ground) belongs to the First Flysch Beds. Weathered limestone on high hill in middle/right background belongs to Thin Platy Limestone Beds. White limestone on upper left is Thick White Limestone Beds.

Figure FT25. Outcrop character of Chert Series Beds.

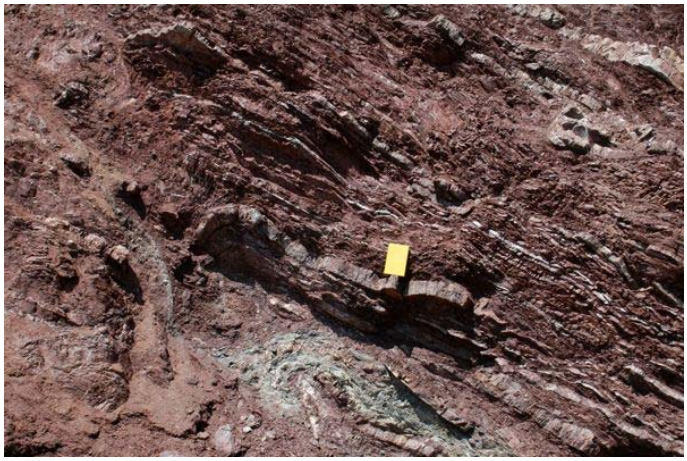

Photograph of roadcut exposure of thrust-faulted and folded beds of limestone, mudstone, and ribbon cherts within the Chert Series Beds. This exposure is in the immediate hanging wall of the Lykaion thrust fault.

As the road continues to climb, it will pass through the Chert Series Beds into First Flysch Beds, composed of massive brown sandstone (Figure FT-26). In the midst of the sandstone outcrops there is an interval of red mudstone, the middle member of the First Flysch Beds. Then

there is a return to outcrops of massive brown sandstone as the road continues to climb.

Figure FT26. Outcrop character of First Flysch Beds.

Photograph of typical outcrop of brown sandstone, the dominant lithology within the First Flysch Beds.

Continuing up the stratigraphic section within the St. Elijah klippe, the next change in formation is the appearance of Thin Platy Limestone Beds (see Figures FT-1, 2). It occurs at the 0.9 km mark, at the beginning of the sharp hairpin bend in the road, i.e., where the direction of travel up the mountain changes from south to north. The roadcut exposures of Thin Platy Limestone Beds display thin beds of limestone, concordant layers and lenses of chert, closely spaced jointing, and tight overturned folding (Figure FT-27).

Figure FT27. Outcrop expression of Thin Platy Limestone Beds.

East-directed photography of roadcut and hillslope exposures of Thin Platy Limestone Beds. The roadcut reveals thin bedding and the presence of white chert layers. The abrupt change in orientation from moderately steeply dipping to gently dipping reflects faulting. Hillslope above the roadcut displays the typical weathered landscape of Thin Platy Limestone Beds.

The next geological change along the road is the appearance of Thick White Limestone Beds (see Figures FT-1, 2). This occurs as the road crosses Grassline fault, the location of which is easy to spot at approximately the 1.1 km mark from Station F (see Figure 38, accompanying manuscript). The trace of the fault coincides with the deep ravine whose head is right at the road, on the right side. The northward trace of Grassline fault is expressed nicely in the landscape, where the smooth narrow field which may be a stadium(?) is evident on the left (see Figure 38).

Finally, take the road to the end, to the ~1.4 km mark, and park at Stop G (see Figures FT-1, 2), which is in the flat area of the temenos, now used as a parking area by those visiting the mountaintop (Figure FT-28).

Figure FT28. Temenos area.

Southeast-directed photograph of temenos area of upper sanctuary. The featureless flat grassy area is part of the temenos. The bold limestone outcrops belong to the Thick White Limestone Beds. Photograph taken from the slope of the ash altar hill.

Stop G.

The contact between Thin Platy Limestone Beds and Thick White Limestone Beds runs essentially along the northern edge of the temenos (see Figures FT-2 and FT-28), which is the trace of the Temenos fault. Along the southern margin of the temenos are low outcrops of Thick White Limestone Beds. One of these outcrop areas appears to be the site of a tiny ancient quarry, for it seems obvious that joint-bounded blocks of the thick-bedded

limestone were removed. Within the temenos area, bedrock is gently dipping, and the stratigraphic level is very close to the depositional contact between Thin Platy Limestone Beds (below) and Thick White Limestone Beds (above). [Section VII-D2 of the companion paper provides descriptions of "Active Faulting within the St. Elijah Klippe"].

The summit of Agios Elias is the rounded hill immediately north of the temenos (Figure FT-29); this is the top of the St. Elijah klippe. The ash altar is on top of this hill. The hill is underlain by Thin Platy Limestone Beds, which weathers and erodes to a smooth, rubbly, grassy hill. Yet in places there are the linear scree bands that mark the traces of active normal faults. One of these is the Altar fault.

Figure FT29. Temenos bordered by active Temenos fault.

Northwest-directed photograph of ash altar hill. Flat foreground is part of the temenos. Flagged rectangle of dirt is archaeological trench. Limestone scree band marks part of the trace of the Temenos fault. Survey instrument on summit is set up close to the ash altar itself. Bedrock underlying ash altar hill is Thin Platy Limestone Beds.

It is satisfying to walk just beyond the eastern edge of the temenos, where the column bases described by Pausanias are still in place (Figure FT-30). Standing between these column bases and looking east, you see a framing of several distinctive steep-sided hilltops, including the spire-like hilltop on which sits the Chapel of St. George. Beyond is the Megalopolis basin.

Figure FT30. Column bases at top of Agios Elias.

Northerly view from eastern edge of temenos showing column bases. On clear days, views of the Peloponessus from the upper sanctuary are grand.

A walk to the top of the ash altar is in order, for on clear days there are breathtaking views of much of the Peloponessus. The Temple of Apollo at Bassai is only ~5 km away, and can be seen off to the west.

It is useful to look at the trace of the Grassline fault from the vantage of the ash altar summit. It is clear that the trace of the fault, marked by scree bands, hugs the base of the north-south trending ridge west of the stadium(?) (see Figure FT-31). The field east of the stadium(?) is marked by alignments of limestone blocks, resembling imperfect traces of ancient walls or seating.

Finally, from the top of Agios Elias, you can look northward and see the hippodrome area, the processional way, and even the location of the bath (Figure FT-32). The scale of the geographic relationships of the upper and lower sanctuary is difficult to grasp, except by walking down to the hippodrome from the ash altar. Along the way you will go in and out of several of the rock formations, which in this part of the mountain are faulted. For someone accustomed to hiking, this excursion can be accomplished leisurely in 45 minutes or less. I recommend it, providing that you do not have to hike back up to return to your vehicles.

Figure FT31. Grassy Fault Trace

A. Southwest-directed view of Grassy fault trace. Hill on right is footwall Thin Platy Limestone Beds. Rock on right of grassy strip is Thick White Limestone Beds.

B. South-directed view of grassy strip along the trace of the Grassy fault. The flatness and softness of this straight-line rectangular strip invites the interpretation that this may have been the site of an early stadium. David Romano, personal communication, 2004.

Figure FT32. View from ash altar to lower sanctuary.

North-directed view down a part of the steep northern slope of the St. Elijah klippe, from ash altar hill to the lower sanctuary and beyond. The trace of the road approximately follows the trace of the Lykaion thrust fault, cutting above it and below it from place to place. The white limestone in the vicinity of the road belongs to Flysch Transition Beds, which occupies the top of the Pan thrust sheet. Above it are the red-purple and brown rocks of the Chert Series Beds and First Flysch Beds in the overlying Zeus thrust sheet. The processional way is in the left center middle ground, and marked by Flysch Transition Beds. The hippodrome is nestled between the processional way and another ridge to the east. Note the cinder track, part of the hippodrome area. Limestone in the background is underlain by Thick White Limestone Beds. The baths are visible in upper left, near the interface between the flat ground and the limestone-bedrock hills.

Table 1

Directions to Stop A from Megalopolis

- Start from SW corner of central square in Megalopolis
- Drive 0.34 km northwest, and take 4th left, which angles west-northwest
- Follow road 1.21 km, where road bends left (west)
- Continue for 0.65 km, where road bends right (north-northwest)
- Continue for 0.44 km, where road bends left (west)
- Continue for 1.75 km, where road bends right (north-northwest)
- Continue for 0.18 km (passing over coal conveyor belts), where road bends sharply left (west-southwest)
- Continue for 0.20 km, where road bends sharply right (north-northwest)

- Continue for 0.35 km, where road forks; take for to left (northwest)
- Continue 0.20 km, where road bends sharply right (north)
- Continue 0.09 km, where road bends sharply left (west-northwest)
- Continue 0.43 km, where road (now in middle of tiny village) bends left (west)
- Continue 0.08 km, where road bends slightly right (west-northwest)
- Continue 0.11 km, where road bends slightly left (west)
- Continue 0.36 km, where road bends slightly left (west-northwest)
- Continue 0.21 km, where road bends right (west-northwest)
- Continue 0.13 km, where road turns sharply left (southwest)
- Continue 0.17 km, where road turns slightly right (west-southwest)
- Continue 0.11 km, where road turns sharply right (north) under conveyor belt
- Continue 0.31 km, where road turns sharply left (west)
- Continue 0.10 km, where road curves sharply left (south)
- Continue 0.08 km, where road curves right (west)
- Continue 0.31 km (road curves broadly westward), where road turns left (south-southwest)
- Continue 0.13 km, where road turns right (west-southwest)
- Continue 0.34 km (through a tiny village), where road bends left (southwest)
- Continue 0.28 km, where road comes to a fork. Take right fork (to west)
- Continue 0.16 km, and take left turn (to southwest)
- Continue 0.14 km, where road comes to a fork. Take right fork (to west-northwest)
- Continue 0.08 km, and keep left (west-southwest) at yet another (small) fork
- Continue 0.35 km, where road bends slightly right (west-northwest)
- Continue 1.95 km, where road bends sharply right (north)
- Continue 0.09 km, where road bends left (northwest)
- Continue 0.06 km, and take the sharp left turn (southwest). You now head steeply up the mountain and will go around ** switchbacks.
- Continue 0.45 km south-southwest to south, to the first switchback, there turning tightly left
- Continue 0.53 in broad arc from northeast to east to south, to the second switchback, there turning tightly right
- Continue 0.27 north-northwest to the third switchback, there turning tightly left
- Continue 0.28 south to the fourth switchback, there turning tightly right
- Continue 0.13 km north-northwest to the fifth switchback, there turning tightly left
- Continue 0.18 km southward, where road turns slightly left (southeast)
- Continue southeast 0.13 km to the sixth switchback, there turning tightly right
- Continue northwest 0.24 km, where road turns sharply west (southwest)
- Continue southwest 0.29 km, where road turns sharply right (northwest)
- Continue northwest 0.1 km, where road turns left (west)
- Continue westward 0.07 km, where road turns sharply right (north-northeast) at spring.
- Continue north-northeast to north for 0.25 km, where road turns right slightly (north-northeast)
- Continue north-northeast 0.12 km. You approach “mirrors” placed at bend (to check for on-coming traffic at the blind curve), and when safe turn tightly left (west)
- Proceed westward for 0.16 km to Stop A, just west of Kastanochori

B. Additional Information on the Stratigraphy

Below are descriptions of the stratigraphy as published by Lalechos (1973) for the Kato Fighalia Sheet and by Papadopoulos (1997) for the Megalopolis Sheet. Observations on the paleontology were provided by Lalechos' colleague, Dr. G. Christodoulou, and by Papadopoulos' colleagues, Dr. S. Tsaila-Monopolis and Dr. V. Skourtsis-Coroneou.

Chert Series consists of thin-bedded multi-colored radiolarian cherts alternating (particularly in the lower part of the formation) with fine-grained sandstones. Upwards within the formation coarse-grained sandstones eventually dominate, yet are interbedded with radiolarian cherts, red marls, and limestones. Thickness of the Chert Series is approximately 100 m. Characteristic fossils are *Pithonella, Globotruncanidae, Orbitolina, Lagenidae, Miliolidae, Textulariidae, and Radiolaria.* The Chert Series is Upper Jurassic to Lower Cretaceous.

First Flysch consists of brown sandstone (ranging from fine to coarse grained) with interbeds of red marl, marly limestone, and microbrecciated limestones. Thickness ranges up to 100 m. Characteristic fossils are *Aeolisaccus kotori, Moncharmontia appenninica, Marginotruncana marginata, Helvetoglobotruncana, Pithonella ovalis, Pithonella, Hedbergella, Heterohelicidae, Hedbergellinae, Orbitolina, Orbitolina concave, Nezzazata, Rotalipora, Pseudocyclammina, and Bacinella irregularis.* First Flysch is Upper Cretaceous, Cenomanian to Lower Turonian.

Limestones are platy to bedded, multicolored, and with layers and nodules of red-black chert. Toward the top of this formation there are interbedded marls and red mudstones as well as sandstones and limestones. Thickness ranges up to 200 m. Characteristic fossils are *Globotruncanita conica, Globotruncana linneiana, Globotruncanita stuarti, Globotruncana ventricosa, Globotruncanita elevate, Rosita fornicate, Pithonella ovalis, and Globotruncanidae.* Limestones are Upper Cretaceous (Turonian to Maastrictian).

Flysch Transition Beds consist of alternating thin-platy to bedded limestones with layers and nodules of chert, and marly limestones. Progressively upward they transition into mudstones with interbedded marly limestones and massive sandstones. Thickness ranges up to 50 m. Characteristic fossils are *Globigerina, Globorotalia, Discocyclina, Globotrucanita stuarti* (reworked), and *Globtruncana arca* (reworked). Flysch Transition Beds are Paleocene to Eocene.